RADIATION PROPERTIES OF SOURCES INSIDE PHOTONIC CRYSTALS

A THESIS

SUBMITTED TO THE DEPARTMENT OF PHYSICS

AND THE INSTITUTE OF ENGINEERING AND SCIENCE

OF BILKENT UNIVERSITY

IN PARTIAL FULFILLMENT OF THE REQUIREMENTS

FOR THE DEGREE OF

MASTER OF SCIENCE

By

İrfan Bulu

September, 2003

I certify that I have read this thesis and that in my opinion it is fully adequate, in scope and in quality, as a thesis for the degree of Master of Science.

Prof. Dr. Ekmel Özbay (Advisor)

I certify that I have read this thesis and that in my opinion it is fully adequate, in scope and in quality, as a thesis for the degree of Master of Science.

Prof. Dr. Atilla Erçelebi

I certify that I have read this thesis and that in my opinion it is fully adequate, in scope and in quality, as a thesis for the degree of Master of Science.

Assoc. Prof. Dr. Ömer Dağ

Approved for the Institute of Engineering and Science:

Prof. Dr. Mehmet B. Baray
Director of the Institute Engineering and Science

ABSTRACT

RADIATION PROPERTIES OF SOURCES INSIDE PHOTONIC CRYSTALS

İrfan Bulu
M.S. in Physics
Supervisor: Prof. Dr. Ekmel Özbay
September, 2003

The control of spontaneous emission is an important problem both in basic and applied physics. Two main problems arise in the control of emission: enhancement or suppression and angular confinement of radiation. In this work we studied the properties of emission of radiation from a localized microwave source embedded inside a photonic crystal. We showed that by using a photonic crystal it is possible to enhance the emitted power. We achieved up to 22 times enhancement of power at the band edge of the photonic crystal. We also studied the properties of emission of radiation from a source embedded inside a single defect structure and embedded inside a coupled defect structure. Enhanced emission for single defect and coupled defect structures was also observed. Moreover, angular distribution of power from a localized microwave source embedded inside a photonic crystal was studied. Angular confinement was achieved near the band edge of the photonic crystal. Half power beam widths as small as 6 degrees were obtained. This is the smallest half power beam width in the literature obtained by using photonic crystals. We also investigated frequency and size dependence of the angular distribution. We observed that the angular confinement strongly depends on frequency and on the size of the photonic crystal. In fact, we showed that angular confinement could be obtained just at the band edge frequency. In conclusion, our work showed that the problem of controlling the spontaneous emission could be solved at once by using photonic crystals.

Keywords: photonic crystal, radiation, band structure, FDTD, enhanced radiation, spontaneous emission, dipole, group velocity, angular confinement.

ÖZET

RADYASYON KAYNAKLARANIN FOTONİK KRİSTALLER İÇİNDEKİ ÖZELLİKLERİ

İrfan Bulu
Fizik, Yüksek Lisans
Tez Yöneticisi: Prof. Dr. Ekmel Özbay
Eylül, 2003

Kendiliğinden ışımanın kontrolü hem temel fizik hem de uygulamalı fizik açısından önemli bir problemdir. Kendiliğinden ışımanın kontrolünde iki önemli problemle karşılaşmaktayız: ışımanın güçlendirilmesi veya engellenmesi ve de ışımanın dar bir açısal bölgeye sıkıştırılması. Bu çalışmada fotonik kristalin içine yerleştirilen yerleşik bir ışıma kaynağı tarafından yapılan mikro dalga ışımasını inceledik. Fotonik kristal kullanarak ışımayı arttırmanın mümkün olduğunu gösterdik. Fotonik kristalin bant köşesinde 22 kat güçlendirilmiş ışıma elde ettik. Buna ek olarak tek kavite ve çiftleşik kavite yapılarının içine yerleştirilen ışıma kaynakları da incelendi. Tek kavite ve çiftleşik kavite yapıları için de güçlendirilmiş ışıma gözledik. Bunlara ek olarak fotonik kristalin içine yerleştirilmiş olan mikro dalga kaynağı tarafından yapılan ışımanın açısal dağılımını da inceledik. Fotonik kristalin bant köşesinde açısal sıkıştırma elde ettik. 6 derece kadar küçük yarım güç genişlikleri elde ettik. Bu yarım güç genişliği literatürde fotonik kristal kullanarak elde edilmiş en küçük değerdir. Açısal dağılımın frekans ve kristal büyüklüğüne bağımlılığı da incelendi. Açısal sıkıştırma sadece bant köşesinde elde edildi. Sonuç olarak çalışmamız fotonik kristalleri kullanarak ışımanın kontrol edilebileceğini gösterdi.

Anahtar sözcükler: fotonik kristal, radyasyon, band yapısı, FDTD, güçlendirilmiş radyasyon, ani ışıma, dipol, grup hızı, açısal sıkıştırma .

Acknowledgement

I would like to express my gratitude to my supervisor Prof. Dr. Ekmel Özbay for his guidance and help in the supervision of the thesis. His personal and academic virtue greatly shaped my approach to physics and scientific study. I feel lucky to be his student.

I would like to thank to the members of my thesis committee, Prof. Atilla Erçelebi and Assoc. Prof. Ömer Dağ, for reading the manuscript and commenting on the thesis.

I would like to express my special thanks and gratitude to Dr. Mehmet Bayindir, Hümeyra Çağlayan, Ertuğrul Çubukçu and Emine abla.

I am also indebted to my mom, my dad and my brothers for their continuous support and encouragement.

I want to thank to my office mates for preparing a nice environment for studying. I am lucky to share the office place with such nice and hardworking friends. Necmi Bıyıklı, İbrahim Kimukin, Koray Aydın, Turgut Tut, Bayram Bütün, S. Sena Akarca Bıyıklı ...

I also want to thank to all the members of the Physics Department. Prof. Salim Çıracı, Prof. Cengiz Bulutay ...

The effort to understand the universe is one of the very few things that lifts human life a little above the level of farce, and gives it some of the grace of tragedy.

Steven Weinberg

Contents

List of Figures

List of Tables

Chapter 1

Introduction

Existence of band gaps is a common phenomenon for all waves propagating through a periodically arranged potential. The presence of a band gap brings many interesting phenomena. For instance, all of the semiconductor devices we are using now is a consequence of the existence of band gaps for electrons. Fundamentally, band gaps provide means of control of the propagation of electrons.

For electrons the periodic potential is provided by the periodically arranged atoms in a crystal. We shall note that appearance of a band gap for electrons is a consequence of the periodic potential. Band gap for electrons does not arise from the electron-electron interactions; rather it arises from the electron-lattice periodic potential interaction. Since the existence of a band gap is a consequence of the periodic potential it is natural to ask whether there may be band gaps for the electromagnetic waves. The possibility of the existence of band gaps for photons was long ago predicted, as early as 1979 [1]. In the case of photons, the periodic potential is provided by a periodically arranged dielectric constant. In fact the similarities between the Maxwell equations written in an eigenvalue form and the hamiltonian for an electron propagating in a periodic potential is striking [2].

Along with the existence of a band gap, a periodic potential for photons has many interesting implications. One major implication is the introduction

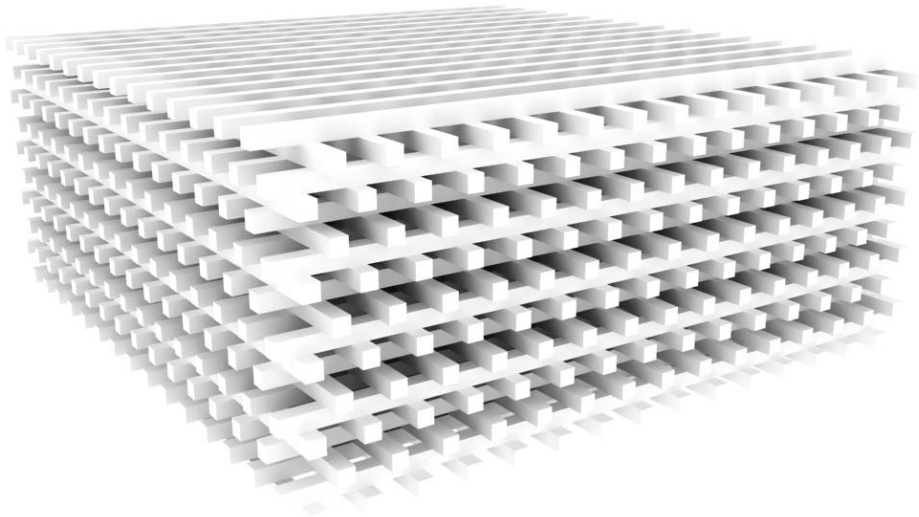

Figure 1.1: A 3 dimensional photonic crystals made from alumina rods. Alumina rods are arranged in a face cubic centered arrangement.

of anisotropy for the dispersion relation of photons. This anisotropy has much far reaching consequences than materials with anisotropic dielectric constants. For instance, it has been shown that negative refraction is possible for photonic crystals. In addition to the anisotropy introduced to the dispersion relation, a periodic dielectric constant arrangement has many interesting implications on wave localization. Localized defect states [3, 4, 5, 6, 7] and coupled cavity waveguides [8, 9, 10, 11, 12, 13] are examples to these implications.

Probably, the most interesting implication of a band gap would be on the interaction between light and localized radiation sources. This was first realized by Yablonovitch [14]. Yablonovitch proposed that structures with periodic dielectric constant arrangement, which we now call photonic crystals, may be used to control the spontaneous emission of radiation. Surprisingly, there are not many experiments related to the control of emission.

What do we mean by the *control* of emission? There are two main important aspects of the *control* of emission: suppression or enhancement of radiation and confinement of the emitted power to a narrow angular region. Suppression of radiation is easily achieved by the presence of a band gap and we are left with two important problems: enhancement and angular confinement. In this thesis, we will show that photonic crystals can be used to solve both problems, enhancement and angular confinement, at once.

Thesis will be organized as follows. In the second chapter, we will have a somewhat long discussion about the theory of photonic crystals and the theory of dipole radiation inside photonic crystals. We will first derive the solutions of Maxwell equations for a periodic medium. Using the solutions of homogeneous Maxwell equations we will obtain the Green's function in terms of an eigenfunction expansion. We will then use the Green's function to solve the problem of emission of radiation from a dipole source embedded inside a photonic crystal. The first chapter will conclude with a brief discussion of FDTD method and the derivation of the reflection and refraction laws for photonic crystals. In the third chapter, we will study the emission of radiation from a source embedded inside a photonic crystal. We will show that the emission of radiation is enhanced near

the upper band edge of the first band gap and at certain defect modes. Moreover, in the third chapter we will analyze the dependence of radiation on the group velocity of the modes and on the source location inside the photonic crystal. Most of the work presented in chapter 3 appeared as a journal article in Physical Review B [15]. In chapter 4, angular distribution of power from a source embedded inside a photonic crystal will be discussed. We will show that a source operating near the band edge of the photonic crystal shows highly directive behavior: The emitted power is confined to a narrow angular region. The results of chapter 4 is to appear as a journal article in Applied Physics Letters [16]. The last chapter will include a brief summary of the results and our future perspective.

Chapter 2

Theoretical Background

In 1946 Purcell [17] predicted the modification of emission of radition from sources by means of electromagnetic mode distribution different from that of the free space electromagnetic mode distribution. This effect has been investigated in cavities with relatively simple structures such as plane mirrors, spheres etc. [18, 19]. Yablonovitch [14] proposed that structures with periodic index modulation, which we now call photonic crystals, can be used to alter the emission of radiation. Periodic dielectric variations lead to the opening of forbidden frequency ranges for electromagnetic waves where no propagation direction is allowed for electromagnetic waves [20, 21, 2, 22].

Radiation properties of sources embedded inside a photonic crystal can be analyzed in terms of the local density of the elecromagnetic eigenmodes (LDOS) [23, 24, 25, 26, 27, 28] and the band structure of the photonic crystal. LDOS for a source embedded inside a photonic crystal depends on certain parameters: group velocity of the eigenmodes, the location of the source inside the photonic crystal, electric field intensity of the eigenmodes at the source location, and the polarization of the source [29, 30, 24, 25, 26, 27, 28]. The power emitted by a source embedded inside a photonic crystal can be adequately described in terms of the LDOS [24, 25, 26, 27, 28]. On the other hand, LDOS does not provide any information on the angular distribution of power emitted by a source embedded inside a photonic crystal. Angular distribution of emitted power can

be analyzed by using the band structure of the photonic crystal i.e., the relation of the direction of the eigenmodes to the eigenfrequencies of the photonic crystal.

In this chapter we will provide the theoretical background for the investigation of photonic crystals and the radiation properties of sources inside photonic crystals. In the first section the calculation of the emitted power in terms of the eigenmodes of the photonic crystal will be given for an infinitesimal dipole embedded inside a photonic crystal. This approach is particularly useful since the method of calculation reveals the properties unique to the photonic crystals and their relation to the emission of power from a source embedded inside a photonic crystal. In this sense the first section will also provide the theoretical background for the photonic crystals. In the second section, a brief discussion of the finite difference time domain method (FDTD) and the calculation of the angular distribution of power by FDTD method will be presented.

2.1 LDOS

LDOS defines the coupling of the source to the electromagnetic modes of the photonic crystal. It can be calculated in terms of the Green's function of the photonic crystal as [23]:

$$\rho(\mathbf{r};\omega) = \frac{-\mathbf{2}\omega}{\pi\mathbf{c^2}}\,\mathbf{Im}[\mathbf{G}(\mathbf{r},\mathbf{r_s};\omega)] \tag{2.1}$$

The Green's function appearing in the definition of LDOS can be calculated by means of eigenfunction expansion. Hence, one needs to convert the Maxwell equations into an eigenvalue problem for the photonic crystal. Once this is done and LDOS is calculated we will see that emission of radiation from a source embedded inside a photonic crystal depends on the group velocity of the eigenmodes of the photonic crystal, the source location, the electric field intensity of the modes at the source location, and the polarization of the source.

In this section we will present the plane wave expansion method to solve the eigenvalue problem for the photonic crystal. Then we will solve the Maxwell equations for an infinitesimal dipole embedded inside a photonic crystal. Finally

calculation of the group velocity of the modes of the photonic crystal by using $k \cdot p$ perturbation method will be presented.

2.1.1 Band structure calculation: the relation between the direction and the frequency of the modes

Maxwell equations for a linear, lossless, charge free, and isotropic medium are:

$$\nabla \cdot \mathbf{D}(\mathbf{r}, \mathbf{t}) = \mathbf{0} \tag{2.2}$$

$$\nabla \cdot \mathbf{B}(\mathbf{r}, \mathbf{t}) = \mathbf{0} \tag{2.3}$$

$$\nabla \times \mathbf{E}(\mathbf{r}, \mathbf{t}) = -\frac{\partial}{\partial \mathbf{t}}\mathbf{B}(\mathbf{r}, \mathbf{t}) \tag{2.4}$$

$$\nabla \times \mathbf{H}(\mathbf{r}, \mathbf{t}) = \frac{\partial}{\partial \mathbf{t}}\mathbf{D}(\mathbf{r}, \mathbf{t}) \tag{2.5}$$

In order to solve these equations we need the equations that relate $\mathbf{B}$ to $\mathbf{H}$ and $\mathbf{D}$ to $\mathbf{E}$. Since the medium is assumed to be linear and isotropic, the relation between $\mathbf{D}$ and $\mathbf{E}$ can be written as:

$$\mathbf{D}(\mathbf{r}, \mathbf{t}) = \varepsilon_{\mathbf{0}}\varepsilon(\mathbf{r})\mathbf{E}(\mathbf{r}, \mathbf{t}) \tag{2.6}$$

Since the medium is assumed to be lossless and linear we have written $\varepsilon(\mathbf{r}, \mathbf{t}) = \varepsilon(\mathbf{r})$ in the above equation.

The dielectric constant for a photonic crystal is a periodic function of the spatial coordinate $\mathbf{r}$:

$$\varepsilon(\mathbf{r} + \mathbf{a_i}) = \varepsilon(\mathbf{r}) \qquad (\mathbf{i} = \mathbf{1}, \mathbf{2}, \mathbf{3}) \tag{2.7}$$

where a_i are the primitive lattice vectors. Since the dielectric function is a periodic function of $\mathbf{r}$ we can represent it as a Fourier series. For the following discussion it is rather useful to expand $1/\varepsilon$ in terms of Fourier coefficients:

$$\frac{1}{\varepsilon(\mathbf{r})} = \Sigma_{\mathbf{G}}\varepsilon(\mathbf{G}) \exp(i\mathbf{G} \cdot \mathbf{r}) \tag{2.8}$$

where $\mathbf{G}$ represents the reciprocal lattice vectors. It is defined as:

$$\mathbf{a}_i \cdot \mathbf{b}_j = 2\pi\delta_{ij} \tag{2.9}$$

$$\mathbf{G} = l_1\mathbf{b}_1 + l_2\mathbf{b}_2 + l_3\mathbf{b}_3 \tag{2.10}$$

For the relation between $\mathbf{B}$ and $\mathbf{H}$ we assume the following relation:

$$\mathbf{B}(\mathbf{r},\mathbf{t}) = \mu_{\mathbf{0}}\mathbf{H}(\mathbf{r}) \tag{2.11}$$

where μ_0 is the magnetic permeability of the free space. This assumption is justified by the fact that we are not dealing with magnetic materials.

Using the constitutive relations 2.6 and 2.11 in the Maxwell equations, we obtain

$$\nabla \cdot \varepsilon(\mathbf{r})\mathbf{E}(\mathbf{r},\mathbf{t}) = 0 \tag{2.12}$$

$$\nabla \cdot \mathbf{H}(\mathbf{r},\mathbf{t}) = \mathbf{0} \tag{2.13}$$

$$\nabla \times \mathbf{E}(\mathbf{r},\mathbf{t}) = -\mu_{\mathbf{0}}\frac{\partial}{\partial \mathbf{t}}\mathbf{B}(\mathbf{r},\mathbf{t}) \tag{2.14}$$

$$\nabla \times \mathbf{H}(\mathbf{r},\mathbf{t}) = \varepsilon_{\mathbf{0}}\varepsilon(\mathbf{r})\frac{\partial}{\partial \mathbf{t}}\mathbf{E}(\mathbf{r},\mathbf{t}) \tag{2.15}$$

To obtain the wave equations we eliminate either $\mathbf{E}$ or $\mathbf{H}$ from the above equations. This can achieved by operating either of the curl equations from the right by the $\nabla\times$ operator. The results are the following wave equations:

$$\tfrac{1}{\varepsilon(\mathbf{r})}\nabla \times \{\nabla \times \mathbf{E}(\mathbf{r},t)\} = -\tfrac{1}{c^2}\tfrac{\partial^2}{\partial t^2}\mathbf{E}(\mathbf{r},t) \tag{2.16}$$

$$\nabla \times \left\{\tfrac{1}{\varepsilon(\mathbf{r})}\nabla \times \mathbf{H}(\mathbf{r},t)\right\} = -\tfrac{1}{c^2}\tfrac{\partial^2}{\partial t^2}\mathbf{H}(\mathbf{r},t) \tag{2.17}$$

If we seek for monochromatic solutions i.e., solutions of the type:

$$\mathbf{E}(\mathbf{r},t) = \mathbf{E}(\mathbf{r})\exp(-i\omega t) \tag{2.18}$$

$$\mathbf{H}(\mathbf{r},t) = \mathbf{H}(\mathbf{r})\exp(-i\omega t) \tag{2.19}$$

we obtain the following equations:

$$\Omega_{\mathbf{E}}\mathbf{E}(\mathbf{r}) = \tfrac{1}{\varepsilon(\mathbf{r})}\nabla \times \{\nabla \times \mathbf{E}(\mathbf{r})\} = \tfrac{\omega^2}{c^2}\mathbf{E}(\mathbf{r}) \tag{2.20}$$

$$\Omega_{\mathbf{H}}\mathbf{H}(\mathbf{r}) = \nabla \times \left\{\tfrac{1}{\varepsilon(\mathbf{r})}\nabla \times \mathbf{H}(\mathbf{r})\right\} = \tfrac{\omega^2}{c^2}\mathbf{H}(\mathbf{r}) \tag{2.21}$$

where ω is the eigen-angular frequency, and $\mathbf{E}(\mathbf{r})$ and $\mathbf{H}(\mathbf{r})$ are the eigen-modes. The operators $\Omega_{\mathbf{E}}$ and $\Omega_{\mathbf{H}}$ are defined as:

$$\Omega_{\mathbf{E}} = \tfrac{1}{\varepsilon(\mathbf{r})}\nabla \times \{\nabla\times\} \tag{2.22}$$

$$\Omega_{\mathbf{H}} = \nabla \times \{\tfrac{1}{\varepsilon(\mathbf{r})}\nabla\times\} \tag{2.23}$$

It is well-known that the solutions of differential equations in the presence of periodic potential terms may be represented in terms of Bloch-functions. Since the potential term $\varepsilon(\mathbf{r})$ is a periodic function of the spatial coordinate $\mathbf{r}$, we can apply the Bloch theorem to the equations 2.18. The solutions of the 2.18 can be written Bloch form as:

$$\mathbf{E}(\mathbf{r}) = \mathbf{E}_{\mathbf{k}n}(\mathbf{r}) = \mathbf{u}_{\mathbf{k}n}(\mathbf{r}) \exp(i\mathbf{k} \cdot r) \tag{2.24}$$

$$\mathbf{H}(\mathbf{r}) = \mathbf{H}_{\mathbf{k}n}(\mathbf{r}) = \mathbf{v}_{\mathbf{k}n}(\mathbf{r}) \exp(i\mathbf{k} \cdot r) \tag{2.25}$$

In the above equations $\mathbf{u}_{\mathbf{k}n}$ and $\mathbf{v}_{\mathbf{k}n}$ are periodic functions of the spatial coordinate $\mathbf{r}$ with the periodicity of the crystal i.e.,

$$\mathbf{u}_{\mathbf{k}n}(\mathbf{r} + \mathbf{a}_i) = \mathbf{u}_{\mathbf{k}n}(\mathbf{r}) \tag{2.26}$$

$$\mathbf{v}_{\mathbf{k}n}(\mathbf{r} + \mathbf{a}_i) = \mathbf{v}_{\mathbf{k}n}(\mathbf{r}) \tag{2.27}$$

Because of the spatial periodicity of the $\mathbf{u}_{\mathbf{k}n}$ and $\mathbf{v}_{\mathbf{k}n}$, these functions can be expanded in Fourier series. Hence $\mathbf{E}_{\mathbf{k}n}$ and $\mathbf{H}_{\mathbf{k}n}$ can be written as:

$$\mathbf{E}_{\mathbf{k}n}(\mathbf{r}) = \textstyle\sum_{\mathbf{G}} \mathbf{E}_{\mathbf{k}n}(\mathbf{G}) \exp(i(\mathbf{k} + \mathbf{G}) \cdot \mathbf{r}) \tag{2.28}$$

$$\mathbf{H}_{\mathbf{k}n}(\mathbf{r}) = \textstyle\sum_{\mathbf{G}} \mathbf{H}_{\mathbf{k}n}(\mathbf{G}) \exp(i(\mathbf{k} + \mathbf{G}) \cdot \mathbf{r}) \tag{2.29}$$

Substituting equation 2.28 into equation 2.20 we obtain the following relations for the Fourier components of $\mathbf{E}_{\mathbf{k}n}$ and $\mathbf{H}_{\mathbf{k}n}$:

$$-\textstyle\sum_{\mathbf{G}'} \varepsilon(\mathbf{G} - \mathbf{G}')(\mathbf{k} + \mathbf{G}') \times \left\{(\mathbf{k} + \mathbf{G}') \times \mathbf{E}_{\mathbf{k}n}(\mathbf{G}')\right\} = \frac{\omega_{\mathbf{k}n}^2}{c^2} \mathbf{E}_{\mathbf{k}n}(\mathbf{G}) \tag{2.30}$$

$$-\textstyle\sum_{\mathbf{G}'} \varepsilon(\mathbf{G} - \mathbf{G}')(\mathbf{k} + \mathbf{G}) \times \left\{(\mathbf{k} + \mathbf{G}') \times \mathbf{H}_{\mathbf{k}n}(\mathbf{G}')\right\} = \frac{\omega_{\mathbf{k}n}^2}{c^2} \mathbf{H}_{\mathbf{k}n}(\mathbf{G}) \tag{2.31}$$

Once we fix $\mathbf{k}$, we obtain one equation of the above type for each reciprocal lattice vector $\mathbf{G}$. These equations can be cast into a matrix form.

$$\begin{pmatrix} & \cdot & \\ & \cdot & \\ -\varepsilon(\mathbf{G}' - \mathbf{G})(\mathbf{k}+\mathbf{G}) \times \{(\mathbf{k}+\mathbf{G})\times\} & & \\ & \cdot & \\ & \cdot & \end{pmatrix} \begin{pmatrix} \cdot \\ \cdot \\ \mathbf{E}_{\mathbf{k}n}(\mathbf{G}) \\ \cdot \\ \cdot \end{pmatrix} = \frac{\omega^2}{c^2} \begin{pmatrix} \cdot \\ \cdot \\ \mathbf{E}_{\mathbf{k}n}(\mathbf{G}) \\ \cdot \\ \cdot \end{pmatrix}$$

$$\begin{pmatrix} & \cdot & \\ & \cdot & \\ -\varepsilon(\mathbf{G}' - \mathbf{G})(\mathbf{k}+\mathbf{G}') \times \{(\mathbf{k}+\mathbf{G})\times\} & & \\ & \cdot & \\ & \cdot & \end{pmatrix} \begin{pmatrix} \cdot \\ \cdot \\ \mathbf{H}_{\mathbf{k}n}(\mathbf{G}) \\ \cdot \\ \cdot \end{pmatrix} = \frac{\omega^2}{c^2} \begin{pmatrix} \cdot \\ \cdot \\ \mathbf{H}_{\mathbf{k}n}(\mathbf{G}) \\ \cdot \\ \cdot \end{pmatrix}$$

These equations define an eigenvalue problem in the infinite dimensional $\mathbf{G}-$*space*. Usually these matrix equations are solved by using usual matrix diagonalization methods for a finite but large set of reciprocal lattice vectors.

Before we present the application of this method to a 2 dimensional photonic crystal it is worth to mention about certain properties of the eigenfunctions and eigenfrequencies.

- $\begin{pmatrix} \mathbf{H}_{n,\mathbf{k}+\mathbf{G}}(\mathbf{r}) \\ \mathbf{E}_{n,\mathbf{k}+\mathbf{G}}(\mathbf{r}) \end{pmatrix} = \begin{pmatrix} \mathbf{H}_{n,\mathbf{k}}(\mathbf{r}) \\ \mathbf{E}_{n,\mathbf{k}}(\mathbf{r}) \end{pmatrix}$
- $\omega_{n,\mathbf{k}+\mathbf{G}} = \omega_{n,\mathbf{k}}$ hence we only need to consider the $\mathbf{k}$ vectors in the first Brillouin zone in our calculations.
- For a set of $3N$ reciprocal lattice vectors we will have $3N$ eigenfrequencies for the solution of $\mathbf{E}_{n,\mathbf{k}}(\mathbf{r})$. On the other hand, we will have $2N$ eigenfrequencies for the solution of $\mathbf{H}_{n,\mathbf{k}}(\mathbf{r})$. This is due to the reduction of the dimension of the matrix used in the solution of $\mathbf{H}_{n,\mathbf{k}}(\mathbf{r})$ by the following condition:

$$\nabla \cdot \mathbf{H}(\mathbf{r}) = \mathbf{0} \tag{2.32}$$

Inserting the Bloch form for $\mathbf{H}(\mathbf{r})$ into this equation we obtain:

$$(\mathbf{k}+\mathbf{G}) \cdot \mathbf{H}_{\mathbf{k}n}(\mathbf{G}) = 0 \tag{2.33}$$

Hence $\mathbf{H}_{\mathbf{k}n}(\mathbf{G})$ is perpendicular to $(\mathbf{k}+\mathbf{G})$ and the matrix dimension is reduced. From this observation we conclude that the N of the eigenvalues have 0 value.

- The group velocity of the modes can be obtained from the band structure of the photonic crystal by the following equation:

$$\mathbf{v_g} = \nabla_{\mathbf{k}}\omega(\mathbf{k}) \tag{2.34}$$

Note that due to the gradient operator in the definition of the group velocity we need to solve the eigenvalue problem for the $\mathbf{k}$ vectors infinitesimally close to the frequency of interest. Instead of the gradient operation we will follow a somewhat indirect method known as the $\mathbf{k}\cdot\mathbf{p}$ perturbation.

We will now apply the method we have just explained to a two dimensional photonic crystal. The crystal is a square array of cylindrical alumina rods. Dielectric constant of the alumina rods is 9.61 and they have a radius of 1.575 mm. The distance between the center of the adjacent rods is 11 mm.

Let us first derive the equations for a two dimensional photonic crystal. For a two dimensional photonic crystal the dielectric constant is uniform in the vertical direction i.e., in the z direction. Hence, $\varepsilon(\mathbf{r})$, $\mathbf{H}(\mathbf{r},t)$ and $\mathbf{E}(\mathbf{r},t)$ are independent of z. It is easy to guess from the form of the Maxwell equations 2.12 that the field equations may be decoupled into two separate set of equations: one set of equations relating the z component of $\mathbf{E}(\mathbf{r},t)$ to the x and y components of $\mathbf{H}(\mathbf{r},t)$, and the other set relating the z component of $\mathbf{H}(\mathbf{r},t)$ to the x and y components of $\mathbf{E}(\mathbf{r},t)$. Since the equations are independent of z coordinate we replace $\mathbf{r}$ with $\mathbf{r}_\parallel$, where $\mathbf{r}_\parallel$ is the 2 dimensional position vector (x,y). The resulting sets of equations are:

$$\frac{\partial}{\partial y}E_z(\mathbf{r}_\parallel,t) = -\mu_0\frac{\partial}{\partial t}H_x(\mathbf{r}_\parallel,t) \tag{2.35}$$

$$\frac{\partial}{\partial x}E_z(\mathbf{r}_\parallel,t) = \mu_0\frac{\partial}{\partial t}H_y(\mathbf{r}_\parallel,t) \tag{2.36}$$

$$\varepsilon_0\varepsilon(\mathbf{r}_\parallel)\frac{\partial}{\partial t}E_z(\mathbf{r}_\parallel,t) = -\frac{\partial}{\partial y}H_x(\mathbf{r}_\parallel,t)+\frac{\partial}{\partial x}H_y(\mathbf{r}_\parallel,t) \tag{2.37}$$

and the other set of equations relating z component of $\mathbf{H}(\mathbf{r},t)$ to the x and y components of $\mathbf{E}(\mathbf{r},t)$ is:

$$\frac{\partial}{\partial y}H_z(\mathbf{r}_\parallel,t) = \varepsilon_0\varepsilon(\mathbf{r}_\parallel)\frac{\partial}{\partial t}E_x(\mathbf{r}_\parallel,t) \quad (2.38)$$

$$\frac{\partial}{\partial x}H_z(\mathbf{r}_\parallel,t) = -\varepsilon_0\varepsilon(\mathbf{r}_\parallel)\frac{\partial}{\partial t}E_y(\mathbf{r}_\parallel,t) \quad (2.39)$$

$$-\mu_0\frac{\partial}{\partial t}H_z(\mathbf{r}_\parallel,t) = -\frac{\partial}{\partial y}E_x(\mathbf{r}_\parallel,t)+\frac{\partial}{\partial x}E_y(\mathbf{r}_\parallel,t) \quad (2.40)$$

By eliminating H_x and H_y from equations 2.35 we obtain the wave equations for E_z and by eliminating E_x and E_y from equations 2.38 we obtain the wave equations for H_z. For E_z:

$$\frac{\partial}{\partial y}(\frac{\partial}{\partial y}E_z(\mathbf{r}_\parallel,t) = -\mu_0\frac{\partial}{\partial t}H_x(\mathbf{r}_\parallel,t)) \quad (2.41)$$

$$\frac{\partial}{\partial x}(\frac{\partial}{\partial x}E_z(\mathbf{r}_\parallel,t) = \mu_0\frac{\partial}{\partial t}H_y(\mathbf{r}_\parallel,t)) \quad (2.42)$$

$$+\text{----------} \quad (2.43)$$

$$(\frac{\partial^2}{\partial y^2}+\frac{\partial^2}{\partial x^2})E_z(\mathbf{r}_\parallel,t) = \mu_0\varepsilon_0\varepsilon(\mathbf{r}_\parallel)\frac{\partial}{\partial t}(\frac{\partial}{\partial x}H_y(\mathbf{r}_\parallel,t)-\frac{\partial}{\partial y}H_x(\mathbf{r}_\parallel,t)) \quad (2.44)$$

Hence,

$$\frac{1}{\varepsilon(\mathbf{r}_\parallel)}(\frac{\partial^2}{\partial y^2}+\frac{\partial^2}{\partial x^2})E_z(\mathbf{r}_\parallel,t) = \frac{1}{c^2}\frac{\partial}{\partial t^2}E_z(\mathbf{r}_\parallel,t) \quad (2.45)$$

For H_z we obtain:

$$(\frac{\partial}{\partial y}\frac{1}{\varepsilon(\mathbf{r}_\parallel)}\frac{\partial}{\partial y}+\frac{\partial}{\partial x}\frac{1}{\varepsilon(\mathbf{r}_\parallel)}\frac{\partial}{\partial x})H_z(\mathbf{r}_\parallel,t) = \frac{1}{c^2}\frac{\partial}{\partial t^2}H_z(\mathbf{r}_\parallel,t) \quad (2.46)$$

Since we can represent any well-behaved function of parameter t as a Fourier series it suffices to consider only the harmonic components i.e.,

$$E_z(\mathbf{r}_\parallel,t) = E_z(\mathbf{r}_\parallel)\exp(-i\omega t) \quad (2.47)$$

$$H_z(\mathbf{r}_\parallel,t) = H_z(\mathbf{r}_\parallel)\exp(-i\omega t) \quad (2.48)$$

Using these forms for E_z and H_z we obtain the following eigenvalue equations:

$$-\frac{1}{\varepsilon(\mathbf{r}_\parallel)}\left\{\frac{\partial^2}{\partial y^2}+\frac{\partial^2}{\partial x^2}\right\}E_z(\mathbf{r}_\parallel) = \frac{\omega^2}{c^2}E_z(\mathbf{r}_\parallel) \quad (2.49)$$

$$-\left\{\frac{\partial}{\partial y}\frac{1}{\varepsilon(\mathbf{r}_\parallel)}\frac{\partial}{\partial y}+\frac{\partial}{\partial x}\frac{1}{\varepsilon(\mathbf{r}_\parallel)}\frac{\partial}{\partial x}\right\}H_z(\mathbf{r}_\parallel) = \frac{\omega^2}{c^2}H_z(\mathbf{r}_\parallel) \quad (2.50)$$

Using the Bloch form for E_z and H_z i.e.,

$$E_z(\mathbf{r}_\parallel) = E_{z,\mathbf{k}_\parallel n}(\mathbf{r}_\parallel) = \sum_{\mathbf{G}_\parallel} E_{z,\mathbf{k}_\parallel n}(\mathbf{G}_\parallel)\exp(i(\mathbf{k}_\parallel + \mathbf{G}_\parallel)\cdot\mathbf{r}_\parallel) \tag{2.51}$$

$$H_z(\mathbf{r}_\parallel) = H_{z,\mathbf{k}_\parallel n}(\mathbf{r}_\parallel) = \sum_{\mathbf{G}_\parallel} H_{z,\mathbf{k}_\parallel n}(\mathbf{G}_\parallel)\exp(i(\mathbf{k}_\parallel + \mathbf{G}_\parallel)\cdot\mathbf{r}_\parallel) \tag{2.52}$$

where $\mathbf{G}_\parallel$ and $\mathbf{k}_\parallel$ represents the 2 dimensional reciprocal lattice vector and the wave vector, we obtain:

$$\sum_{\mathbf{G}'_\parallel} \varepsilon(\mathbf{G}_\parallel - \mathbf{G}'_\parallel)\left|\mathbf{k}_\parallel + \mathbf{G}'_\parallel\right|^2 E_{z,\mathbf{k}_\parallel n}(\mathbf{G}'_\parallel) = \frac{\omega^{(E)2}_{\mathbf{k}n}}{c^2} E_{z,\mathbf{k}_\parallel n}(\mathbf{G}_\parallel) \tag{2.53}$$

$$\sum_{\mathbf{G}'_\parallel} \varepsilon(\mathbf{G}_\parallel - \mathbf{G}'_\parallel)\left(\mathbf{k}_\parallel + \mathbf{G}'_\parallel\right)\cdot\left(\mathbf{k}_\parallel + \mathbf{G}_\parallel\right) H_{z,\mathbf{k}_\parallel n}(\mathbf{G}'_\parallel) = \frac{\omega^{(H)2}_{\mathbf{k}n}}{c^2} H_{z,\mathbf{k}_\parallel n}(\mathbf{G}_\parallel) \tag{2.54}$$

To solve these equations we need to find the Fourier components of the inverse dielectric function for the periodic array of cylindrical rods. Using r_r and $\varepsilon|r$ for the radius and the dielectric constant of the rods, and ε_0 for the background index, we can write down the dielectric function of the medium as:

$$\frac{1}{\varepsilon(\mathbf{r}_\parallel)} = \frac{1}{\varepsilon_0} + \left(\frac{1}{\varepsilon_r} - \frac{1}{\varepsilon_0}\right) S(\mathbf{r}_\parallel) \tag{2.55}$$

$$S(\mathbf{r}_\parallel) = \begin{cases} 1 \;\; for \;\; \left|\mathbf{r}_\parallel\right| \le r_r \\ 0 \;\; for \;\; \left|\mathbf{r}_\parallel\right| > r_r \end{cases} \tag{2.56}$$

Using the Fourier transform,

$$\varepsilon(\mathbf{G}_\parallel) = \frac{1}{A}\int_A d\mathbf{r}_\parallel \frac{1}{\varepsilon(\mathbf{r}_\parallel)}\exp(-i\mathbf{G}_\parallel\cdot\mathbf{r}_\parallel) \tag{2.57}$$

where A is the area of the unit cell, we obtain for the Fourier components $\varepsilon(\mathbf{G}_\parallel)$:

$$\varepsilon(\mathbf{G}_\parallel) = \frac{1}{\varepsilon_0}\delta_{\mathbf{G}_\parallel 0+} \frac{1}{A}\left(\frac{1}{\varepsilon_r} - \frac{1}{\varepsilon_0}\right)\int_A d\mathbf{r}_\parallel S(\mathbf{r}_\parallel)\exp(-i\mathbf{G}_\parallel\cdot\mathbf{r}_\parallel) \tag{2.58}$$

This equation can be evaluated by the help of

$$\exp(i\omega\sin\theta) = \sum_{-\infty}^{\infty} J_l(\omega)\exp(il\theta) \tag{2.59}$$

This representation of Bessel functions is also well-known in the scattering theory. Substituting equation 2.59 into equation 2.58 we obtain:

$$\int_A d\mathbf{r}_\parallel S(\mathbf{r}_\parallel) \exp(-i\mathbf{G}_\parallel \cdot \mathbf{r}_\parallel) = \int_0^{r_r} r dr \int_0^{2\pi} d\varphi \sum_{-\infty}^{\infty} J_l(Gr) \exp(il\left(\varphi - \frac{\pi}{2}\right)) \tag{2.60}$$

$$= 2\pi \int_0^{r_r} r J_0(Gr) dr \tag{2.61}$$

using the following identity,

$$\frac{d}{dr}\left[r J_1(r)\right] = r J_0(r) \tag{2.62}$$

equation 2.61 can be written as:

$$\frac{2\pi r_r}{G} J_1(G r_r) \tag{2.63}$$

Hence, the Fourier components of inverse dielectric constant are:

$$\varepsilon(\mathbf{G}_\parallel) = 2f\left(\frac{1}{\varepsilon_r} - \frac{1}{\varepsilon_0}\right)\frac{J_1(Gr_r)}{Gr_r} \tag{2.64}$$

where f is the filling fraction. for $\varepsilon(0)$ we have

$$\varepsilon(0) = \frac{1}{\varepsilon_r} + \frac{f-1}{\varepsilon_0} \tag{2.65}$$

Now we are in a position to solve the problem of a square array of cylindrical rods we just mentioned.

As we have pointed out in the discussion about the properties of the solutions of the wave equations for a periodic potential it was said that the solutions are periodic in the reciprocal lattice. Hence, we only need to consider the first Brillouin zone.

We will now present the band structure for the $2D$ photonic crystal that we mentioned above. The cylindrical rods are assumed to be infinite in extent along direction parallel to the axis of the rods. It is customary to calculate the band structure along the path $\Gamma \rightarrow X \rightarrow M \rightarrow \Gamma$ shown in Fig. 2.2. The calculated

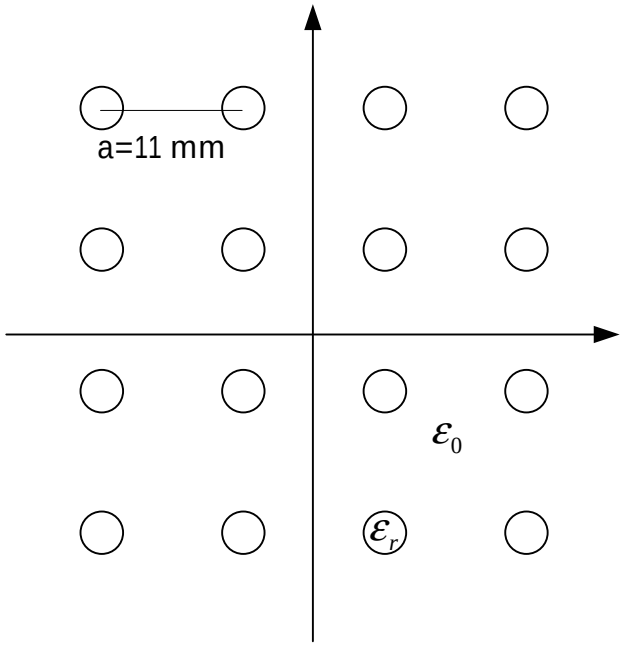

Figure 2.1: Schematics of the $2D$ square array of cylindrical alumina rods.

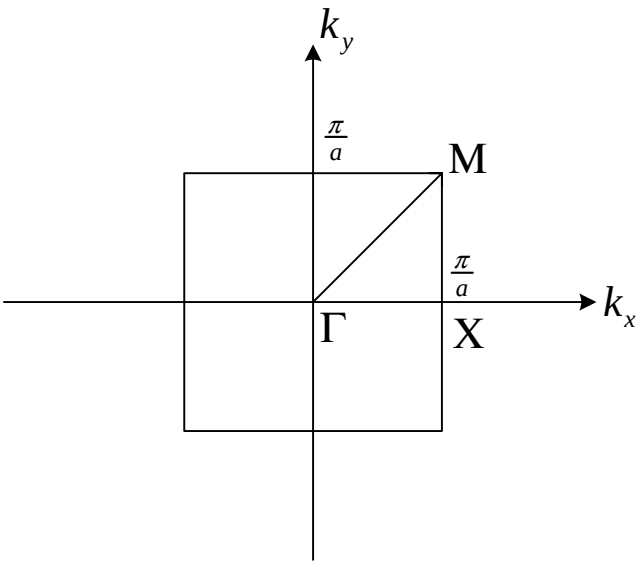

Figure 2.2: The first Brillouin zone for a square lattice. The zone boundaries are $k_x = \mp\frac{\pi}{a}$ and $k_y = \mp\frac{\pi}{a}$.

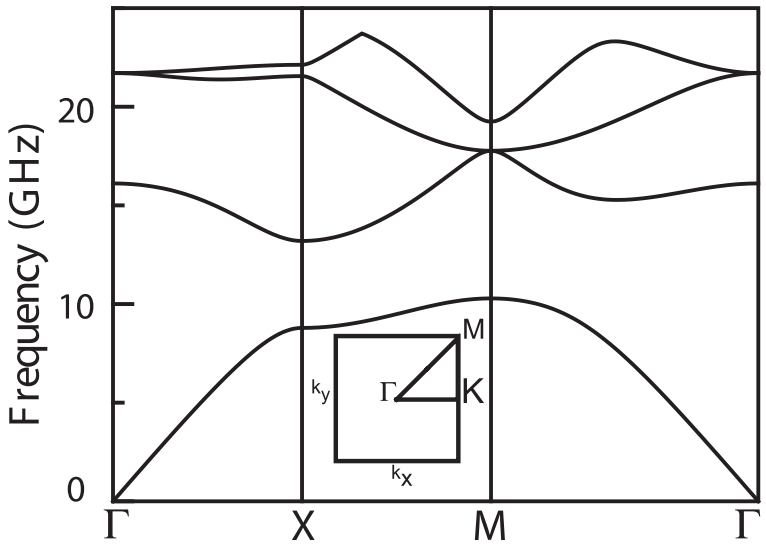

Figure 2.3: Band structure for the square array of the cylindrical rods for TM polarized electromagnetic waves. Eigenvalues are calculated along the path $\Gamma \rightarrow X \rightarrow M \rightarrow \Gamma$.

band structure along the given path is shown in Fig. 2.3. From Fig. 2.3 we observe that there is a frequency range between the first band and second band where no modes are allowed to propagate in the photonic crystal. This range is called the photonic band gap. Actually, it can be shown that the wave vectors of these modes are imaginary. In our case first band gap extends from 10.2 GHz to 13.18 GHz

Electric field intensities of the modes for the first 2 bands at the high symmetry points X and M are shown in Figs. 2.4, and 2.5. In all figures darker the color higher the intensity of electric field. Properties of these modes will be of interest to us in the following chapters. From Figs. 2.4, and 2.5 we observe that for the modes of the first band electric field intensity is higher near the high dielectric region of the photonic crystal. On the other electric field intensity is higher near the low dielectric region of the photonic crystal for the modes of the second band. Actually, the modes of the first band are called dielectric modes and the modes of the second band are called air bands.

At this moment it is worth to mention that up to now we have only calculated the eigenvalues and the eigenfunctions of the Maxwell equations for a periodic

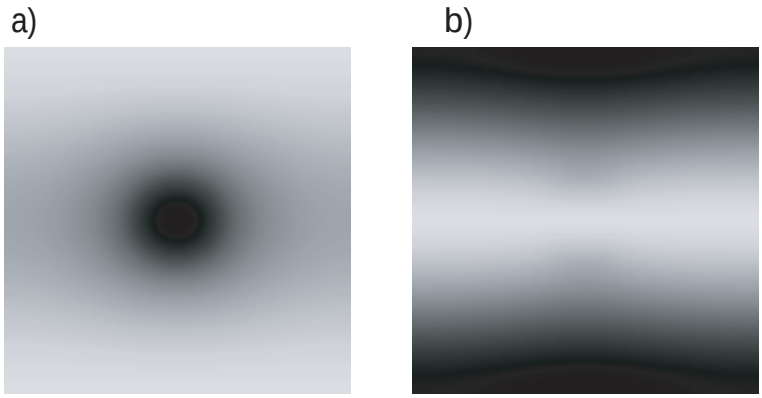

Figure 2.4: a) Electric field intensity for the first eigenmode at X point in the square primitive cell. Electric field is TM polarized in this case. Note that the electric field intensity is higher at the high index regions of the unit cell compared to low index regions. b) Electric field intensity for the second eigenmode at X point in the square primitive cell. Electric field is TM polarized in this case. Note that the electric field intensity is higher at the low index regions of the unit cell compared to high index regions.

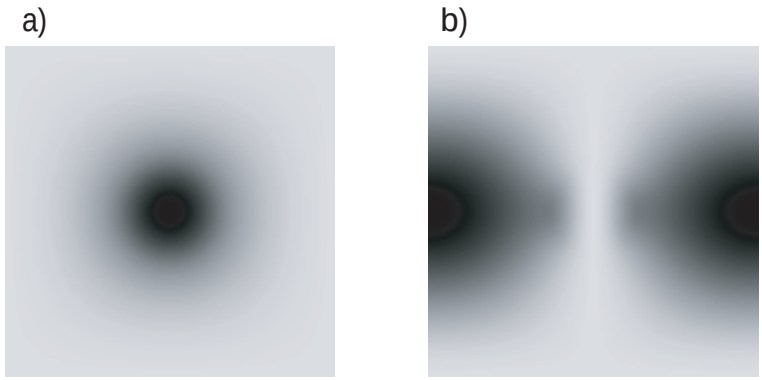

Figure 2.5: a) Electric field intensity for the first eigenmode at M point in the square primitive cell. Electric field is TM polarized in this case. Note that the electric field intensity is higher at the high index regions of the unit cell compared to low index regions. b) Electric field intensity for the second eigenmode at M point in the square primitive cell. Electric field is TM polarized in this case. Note that the electric field intensity is higher at the low index regions of the unit cell compared to high index regions.

dielectric constant modulation. Although the method is very useful for calculating the eigenvalues and eigenfunctions it does not provide much information about the transmission properties of the photonic crystal. The transmission properties of the photonic crystal maybe estimated by considering the density of the modes along a given direction and the overlap between the incident field and the modes of the photonic crystal. There is a more direct approach to the transmission problem. We will come to this point later.

We have calculated the eigenvalues and the eigenfunctions of the Maxwell equations for the photonic crystal. To be able to find the form of the Green's function we need to find the complete set of eigenfunctions. Hence we need to consider the modes with 0 angular frequency. This point will be explained in the following section and the Green's function will be derived in the following section.

2.1.2 Green's function

When expanding the Green's function in terms of the eigenfunctions of an operator we need a complete set of eigenfunction. It is well-known that the eigenfunctions of an Hermitian operator form a complete set of functions. Any function can be expanded in terms of the eigenfunctions of an Hermitian operator. We have calculated the eigenfunctions of the operator

$$\Omega_{\mathbf{E}} = \frac{1}{\varepsilon(\mathbf{r})}\nabla \times \{\nabla \times\} \tag{2.66}$$

in the previous section. Operator $\Omega_{\mathbf{E}}$ is not an Hermitian operator. Hence the set of eigenfunctions $\{\mathbf{E}_{\mathbf{k}n}(\mathbf{r})\}$ does not form a complete set. Hence we need to convert operator $\Omega_{\mathbf{E}}$ to an Hermitian operator. We define:

$$\mathbf{\Xi}(\mathbf{r}, t) = \sqrt{\varepsilon(\mathbf{r})}\mathbf{E}(\mathbf{r}, t) \tag{2.67}$$

We will show that $\mathbf{\Xi}(\mathbf{r})$ satisfies and equation defined by an Hermitian operator. Let us remember the differential equation satisfied by $\mathbf{E}(\mathbf{r}, t)$:

$$\frac{1}{\epsilon(\mathbf{r})}\nabla \times \{\nabla \times \mathbf{E}(\mathbf{r},t)\} = -\frac{1}{c^2}\frac{\partial^2}{\partial t^2}\mathbf{E}(\mathbf{r},t) \tag{2.68}$$

Hence, $\mathbf{\Xi}(\mathbf{r},t)$ satisfies the following differential equation:

$$\left\{\frac{1}{c^2}\frac{\partial^2}{\partial t^2} + \frac{1}{\sqrt{\epsilon(\mathbf{r})}}\nabla \times \left[\nabla \times \frac{1}{\sqrt{\epsilon(\mathbf{r})}}\right]\right\}\mathbf{\Xi}(\mathbf{r},t) = 0 \tag{2.69}$$

As usual we look for the harmonic solutions of eqn. 2.69. We obtain:

$$\frac{1}{\sqrt{\epsilon(\mathbf{r})}}\nabla \times \left[\nabla \times \frac{1}{\sqrt{\epsilon(\mathbf{r})}}\right]\mathbf{\Xi}(\mathbf{r}) = \frac{\omega^2}{c^2}\mathbf{\Xi}(\mathbf{r}) \tag{2.70}$$

We will know show that the operator defined by the left hand side of eqn. 2.70,

$$\Pi = \frac{1}{\sqrt{\epsilon(\mathbf{r})}}\nabla \times \left[\nabla \times \frac{1}{\sqrt{\epsilon(\mathbf{r})}}\right] \tag{2.71}$$

is Hermitian. We need to show that $\Pi = \Pi^{\dagger}$. This is equivalent to:

$$< \mathbf{\Xi}_1(\mathbf{r})\Pi \mid \mathbf{\Xi}_2(\mathbf{r}) >=< \mathbf{\Xi}_1(\mathbf{r}) \mid \Pi\mathbf{\Xi}_2(\mathbf{r}) > \tag{2.72}$$

Let us evaluate the left hand side of eqn. 2.72:

$$< \mathbf{\Xi}_1(\mathbf{r})\Pi \mid \mathbf{\Xi}_2(\mathbf{r}) >= \int_V \left\{\frac{1}{\sqrt{\epsilon(\mathbf{r})}}\nabla \times \left[\nabla \times \frac{1}{\sqrt{\epsilon(\mathbf{r})}}\mathbf{\Xi}_1^*(\mathbf{r})\right]\right\}\mathbf{\Xi}_2(\mathbf{r})d\mathbf{r} \tag{2.73}$$

using the following identity in eqn. 2.74,

$$\nabla \cdot (\mathbf{A} \times \mathbf{B}) = (\nabla \times \mathbf{A}) \cdot \mathbf{B} - \mathbf{A}.(\nabla \times \mathbf{B}) \tag{2.74}$$

we obtain:

$$\begin{aligned} & \left\{ \nabla \times \left[\nabla \times \frac{1}{\sqrt{\epsilon(\mathbf{r})}} \mathbf{\Xi}_1^*(\mathbf{r}) \right] \right\} \frac{\mathbf{\Xi}_2(\mathbf{r})}{\sqrt{\epsilon(\mathbf{r})}} \\ = & \left[\nabla \times \frac{1}{\sqrt{\epsilon(\mathbf{r})}} \mathbf{\Xi}_1^*(\mathbf{r}) \right] \cdot \left[\nabla \times \frac{1}{\sqrt{\epsilon(\mathbf{r})}} \mathbf{\Xi}_2(\mathbf{r}) \right] + \nabla \cdot \left\{ \left[\nabla \times \frac{1}{\sqrt{\epsilon(\mathbf{r})}} \mathbf{\Xi}_1^*(\mathbf{r}) \right] \times \frac{\mathbf{\Xi}_2(\mathbf{r})}{\sqrt{\epsilon(\mathbf{r})}} \right\} \end{aligned}$$

Hence, eqn. 2.73 can be written as:

$$= \int_{\mathbf{A}} d\mathbf{A} \cdot \left\{ \left[\nabla \times \frac{1}{\sqrt{\epsilon(\mathbf{r})}} \mathbf{\Xi}_1^*(\mathbf{r}) \right] \times \frac{\mathbf{\Xi}_2(\mathbf{r})}{\sqrt{\epsilon(\mathbf{r})}} \right\} + \int_V \left[\nabla \times \frac{1}{\sqrt{\epsilon(\mathbf{r})}} \mathbf{\Xi}_1^*(\mathbf{r}) \right] \cdot \left[\nabla \times \frac{1}{\sqrt{\epsilon(\mathbf{r})}} \mathbf{\Xi}_2(\mathbf{r}) \right] \tag{2.75}$$

The surface integral vanishes. This is because since $\mathbf{E}(\mathbf{r})$ can be written in the Bloch form, $\mathbf{\Xi}(\mathbf{r})$ is subject to the boundary conditions. Applying once more the vector identity given by eqn. 2.74 we obtain:

$$\begin{aligned} & \int_V \left[\nabla \times \frac{1}{\sqrt{\epsilon(\mathbf{r})}} \mathbf{\Xi}_1^*(\mathbf{r}) \right] \cdot \left[\nabla \times \frac{1}{\sqrt{\epsilon(\mathbf{r})}} \mathbf{\Xi}_2(\mathbf{r}) \right] \\ = & \int_{\mathbf{A}} d\mathbf{A} \cdot \left\{ \frac{\mathbf{\Xi}_1^*(\mathbf{r})}{\sqrt{\epsilon(\mathbf{r})}} \times \left[\nabla \times \frac{1}{\sqrt{\epsilon(\mathbf{r})}} \mathbf{\Xi}_2(\mathbf{r}) \right] \right\} + \int_V \frac{\mathbf{\Xi}_1^*(\mathbf{r})}{\sqrt{\epsilon(\mathbf{r})}} \cdot \left\{ \nabla \times \left[\nabla \times \frac{1}{\sqrt{\epsilon(\mathbf{r})}} \mathbf{\Xi}_2(\mathbf{r}) \right] \right\} \end{aligned}$$

The surface integral vanishes. This result implies:

$$< \mathbf{\Xi}_1(\mathbf{r}) \Pi \mid \mathbf{\Xi}_2(\mathbf{r}) > = < \mathbf{\Xi}_1(\mathbf{r}) \mid \Pi \mathbf{\Xi}_2(\mathbf{r}) > \tag{2.76}$$

Hence the operator Π is hermitian and the eigenfunctions of Π form a complete set. Also note that the eigenfunctions of an Hermitian operator are orthogonal to each other.

In the previous section we have found out that N of $3N$ eigenvalues $\omega_{\mathbf{k}n}$ are 0. There is one such solution for each $\mathbf{k}$ and for each band i.e., we must have solutions satisfying the following equation:

$$\nabla \times \mathbf{E}_{\mathbf{k}n}(\mathbf{r}) = 0 \tag{2.77}$$

Using the Bloch form for $\mathbf{E}_{\mathbf{k}n}(\mathbf{r})$, condition 2.77 can written as:

$$\nabla \times \left\{ \sum_{\mathbf{G}} \mathbf{E}_{\mathbf{k}n}(\mathbf{G}) \exp(i(\mathbf{k}+\mathbf{G}) \cdot \mathbf{r}) \right\} = \sum_{\mathbf{G}} i(\mathbf{k}+\mathbf{G}) \times \mathbf{E}_{\mathbf{k}n}(\mathbf{G}) \exp(i(\mathbf{k}+\mathbf{G}) \cdot \mathbf{r}) = 0 \tag{2.78}$$

Equation 2.78 implies that:

$$\mathbf{E}_{\mathbf{k}n}(\mathbf{G}) \propto \mathbf{k}+\mathbf{G} \tag{2.79}$$

Denoting the solutions with 0 eigenvalue as:

$$\mathbf{E}^{(L)}_{\mathbf{k}n} \tag{2.80}$$

We can write $\mathbf{\Xi}^{(L)}_{\mathbf{k}n}$ as:

$$\mathbf{\Xi}^{(L)}_{\mathbf{k}n}(\mathbf{r}) = C\sqrt{\epsilon(\mathbf{r})} \frac{\mathbf{k}+\mathbf{G}}{|\mathbf{k}+\mathbf{G}|} \exp(i(\mathbf{k}+\mathbf{G}) \cdot \mathbf{r}) \tag{2.81}$$

This particular form is chosen to ensure the orthogonality of $\mathbf{\Xi}^{(L)}_{\mathbf{k}n}$ with different $\mathbf{k}n$. $\mathbf{\Xi}^{(L)}_{\mathbf{k}n}$ satisfies the following equation:

$$\nabla \times \left\{ \frac{1}{\sqrt{\epsilon(\mathbf{r})}} \mathbf{\Xi}^{(L)}_{\mathbf{k}n}(\mathbf{r}) \right\} = 0 \tag{2.82}$$

Since the eigenfunctions of operator Π form a complete set, by denoting the eigenfunctions of Π with eigenvalue different than 0 as $\mathbf{\Xi}^{(T)}_{\mathbf{k}n}$, we can write:

$$\sum_{\mathbf{k}n} \mathbf{\Xi}^{(L)}_{\mathbf{k}n}(\mathbf{r}) \otimes \mathbf{\Xi}^{(L)*}_{\mathbf{k}n}(\mathbf{r}^{'}) + \sum_{\mathbf{k}n} \mathbf{\Xi}^{(T)}_{\mathbf{k}n}(\mathbf{r}) \otimes \mathbf{\Xi}^{(T)*}_{\mathbf{k}n}(\mathbf{r}^{'}) = V \overleftrightarrow{I}\, \delta(\mathbf{r} - \mathbf{r}^{'}) \tag{2.83}$$

where $(\mathbf{A} \otimes \mathbf{B})_{ij} = A_i B_j$ and $\overleftrightarrow{I}$ is the unit tensor.

This representation of dirac-delta function is particularly useful in deriving the Green's function in terms of an eigenfunction expansion.

We are now in a position to derive the Green's function. Green's function satisfies the following differential equation:

$$\left\{ \frac{1}{c^2} \frac{\partial^2}{\partial t^2} + \Pi \right\} \overleftrightarrow{G}(\mathbf{r}, \mathbf{r}^{'}, t - t^{'}) = - \overleftrightarrow{I}\, \delta(\mathbf{r} - \mathbf{r}^{'}) \delta(t - t^{'}) \tag{2.84}$$

The time dependent Green's function can be written as a Fourier transform in the frequency space. If

$$\overleftrightarrow{G}(\mathbf{r}, \mathbf{r}^{'}, t - t^{'}) \quad \text{for} \quad t < 0$$

then

$$\overleftrightarrow{G}(\mathbf{r}, \mathbf{r}^{'}, t) = \frac{1}{\sqrt{2\pi}} \int_{-\infty}^{\infty} \overleftrightarrow{G}(\mathbf{r}, \mathbf{r}^{'}, \omega) \exp(-i\omega t) d\omega \tag{2.85}$$

and

$$\overleftrightarrow{G}(\mathbf{r}, \mathbf{r}^{'}, \omega) = \frac{1}{\sqrt{2\pi}} \int_{-\infty}^{\infty} \overleftrightarrow{G}(\mathbf{r}, \mathbf{r}^{'}, t) \exp(i\omega t) dt \tag{2.86}$$

Note that we have used the symmetric representation of the Green's function. If we Fourier transform eqn. 2.84, we obtain:

$$\left\{\frac{\omega^2}{c^2} - \Pi\right\} \overleftrightarrow{G}(\mathbf{r}, \mathbf{r}', \omega) = \overleftrightarrow{I}\,\delta(\mathbf{r} - \mathbf{r}') \tag{2.87}$$

This equation can be solved by the fact that:

$$\mathbf{\Pi\Xi}^{(T)}_{\mathbf{k}n}(\mathbf{r}) = \frac{\omega^{(T)2}_{\mathbf{k}n}}{c^2}\mathbf{\Xi}^{(T)}_{\mathbf{k}n}(\mathbf{r}) \tag{2.88}$$

and

$$\mathbf{\Pi\Xi}^{(L)}_{\mathbf{k}n}(\mathbf{r}) = 0 \tag{2.89}$$

and eqn. 2.83, we obtain:

$$\overleftrightarrow{G}(\mathbf{r}, \mathbf{r}', \omega) = \frac{c^2}{\sqrt{2\pi}V}\sum_{\mathbf{k}n}\left\{\frac{\mathbf{\Xi}^{(T)}_{\mathbf{k}n}(\mathbf{r}) \otimes \mathbf{\Xi}^{(T)*}_{\mathbf{k}n}(\mathbf{r}')}{\left(\omega - \omega^{(T)}_{\mathbf{k}n} + i\delta\right)\cdot\left(\omega + \omega^{(T)}_{\mathbf{k}n} + i\delta\right)} + \frac{\mathbf{\Xi}^{(L)}_{\mathbf{k}n}(\mathbf{r}) \otimes \mathbf{\Xi}^{(L)*}_{\mathbf{k}n}(\mathbf{r}')}{(\omega + i\delta)^2}\right\} \tag{2.90}$$

Here δ is a positive infinitesimal. Its role is to ensure the causality. To find the time dependent Green's function we use the inverse Fourier transform given by eqn. 2.86:

$$\overleftrightarrow{G}(\mathbf{r}, \mathbf{r}', t) = \frac{1}{\sqrt{2\pi}}\int_{-\infty}^{\infty}\overleftrightarrow{G}(\mathbf{r}, \mathbf{r}', \omega)\exp(-i\omega t)d\omega$$

$$= \frac{c^2}{2\pi V}\int_{-\infty}^{\infty}\left[\sum_{\mathbf{k}n}\left\{\frac{\mathbf{\Xi}^{(T)}_{\mathbf{k}n}(\mathbf{r}) \otimes \mathbf{\Xi}^{(T)*}_{\mathbf{k}n}(\mathbf{r}')}{\left(\omega - \omega^{(T)}_{\mathbf{k}n} + i\delta\right)\cdot\left(\omega + \omega^{(T)}_{\mathbf{k}n} + i\delta\right)} + \frac{\mathbf{\Xi}^{(L)}_{\mathbf{k}n}(\mathbf{r}) \otimes \mathbf{\Xi}^{(L)*}_{\mathbf{k}n}(\mathbf{r}')}{(\omega + i\delta)^2}\right\}\right]\exp(-i\omega t)$$

since

$$\frac{\mathbf{\Xi}_{\mathbf{k}n}^{(T)}(\mathbf{r}) \otimes \mathbf{\Xi}_{\mathbf{k}n}^{(T)*}(\mathbf{r}')}{\left(\omega - \omega_{\mathbf{k}n}^{(T)} + i\delta\right) \cdot \left(\omega + \omega_{\mathbf{k}n}^{(T)} + i\delta\right)} = \left\{ \frac{\mathbf{\Xi}_{\mathbf{k}n}^{(T)}(\mathbf{r}) \otimes \mathbf{\Xi}_{\mathbf{k}n}^{(T)*}(\mathbf{r}')}{2\omega_{\mathbf{k}n}^{(T)}} \right\} \left(\frac{1}{\omega - \omega_{\mathbf{k}n}^{(T)} + i\delta} - \frac{1}{\omega + \omega_{\mathbf{k}n}^{(T)} + i\delta} \right)$$

we obtain:

$$= \frac{c^2}{2\pi V} \sum_{\mathbf{k}n} \left\{ \frac{\mathbf{\Xi}_{\mathbf{k}n}^{(T)}(\mathbf{r}) \otimes \mathbf{\Xi}_{\mathbf{k}n}^{(T)*}(\mathbf{r}')}{2\omega_{\mathbf{k}n}^{(T)}} \right\} \int_{-\infty}^{\infty} \left(\frac{1}{\omega - \omega_{\mathbf{k}n}^{(T)} + i\delta} - \frac{1}{\omega + \omega_{\mathbf{k}n}^{(T)} + i\delta} \right) \exp(-i\omega t) d\omega$$

$$+ \frac{c^2}{2\pi V} \sum_{\mathbf{k}n} \mathbf{\Xi}_{\mathbf{k}n}^{(L)}(\mathbf{r}) \otimes \mathbf{\Xi}_{\mathbf{k}n}^{(L)*}(\mathbf{r}') \int_{-\infty}^{\infty} \frac{1}{(\omega + i\delta)^2} \exp(-i\omega t) d\omega$$

This rather cumbersome equation is easy to evaluate the method of residues:

$$= \frac{c^2}{2\pi V} \sum_{\mathbf{k}n} \left\{ \frac{\mathbf{\Xi}_{\mathbf{k}n}^{(T)}(\mathbf{r}) \otimes \mathbf{\Xi}_{\mathbf{k}n}^{(T)*}(\mathbf{r}')}{2\omega_{\mathbf{k}n}^{(T)}} \right\} \int_{C} \left(\frac{1}{\omega - \omega_{\mathbf{k}n}^{(T)} + i\delta} - \frac{1}{\omega + \omega_{\mathbf{k}n}^{(T)} + i\delta} \right) \exp(-i\omega t) d\omega$$

$$+ \frac{c^2}{2\pi V} \sum_{\mathbf{k}n} \mathbf{\Xi}_{\mathbf{k}n}^{(L)}(\mathbf{r}) \otimes \mathbf{\Xi}_{\mathbf{k}n}^{(L)*}(\mathbf{r}') \int_{C} \frac{1}{(\omega + i\delta)^2} \exp(-i\omega t) d\omega$$

In this case ω is a considered as a complex number. For $t \geq 0$ we can use a half-circle in lower complex half plane. And if the radius of the circle $C_r \to \infty$ we obtain:

$$\int_{C} \left(\frac{1}{\omega - \omega_{\mathbf{k}n}^{(T)} + i\delta} - \frac{1}{\omega + \omega_{\mathbf{k}n}^{(T)} + i\delta} \right) \exp(-i\omega t) d\omega = -4\pi \sin(\omega_{\mathbf{k}n}^{(T)} t)$$

and

$$\int_C \frac{1}{(\omega + i\delta)^2} \exp(-i\omega t) d\omega = -2\pi t$$

Finally, we can write the time dependent Green's function as:

$$\overleftrightarrow{G}(\mathbf{r}, \mathbf{r}', t) = -\frac{c^2}{V} \sum_{\mathbf{k}n} \left\{ \mathbf{\Xi}^{(T)}_{\mathbf{k}n}(\mathbf{r}) \otimes \mathbf{\Xi}^{(T)*}_{\mathbf{k}n}(\mathbf{r}') \frac{\sin(\omega^{(T)}_{\mathbf{k}n} t)}{\omega^{(T)}_{\mathbf{k}n}} + t \mathbf{\Xi}^{(L)}_{\mathbf{k}n}(\mathbf{r}) \otimes \mathbf{\Xi}^{(L)*}_{\mathbf{k}n}(\mathbf{r}') \right\} \tag{2.91}$$

For the 2 dimensional problem since the Maxwell equations are decoupled into two separate sets of equations one for TM polarized waves, electric field is parallel to the axis of rods, and one for TE polarized waves, magnetic field is parallel to the axis of the rods, we can define:

$$\mathbf{\Xi}^{(TM)}(\mathbf{r}, t) = \sqrt{\varepsilon(\mathbf{r}_\parallel)} \mathbf{E}_z(\mathbf{r}_\parallel, t) \tag{2.92}$$

$$\mathbf{\Pi}^{(TM)} = -\frac{1}{\sqrt{\epsilon(\mathbf{r}_\parallel)}} \left(\frac{\partial^2}{\partial y^2} + \frac{\partial^2}{\partial x^2} \right) \frac{1}{\sqrt{\epsilon(\mathbf{r}_\parallel)}} \tag{2.93}$$

We consider TM polarized waves, since we will be concerned with TM polarized waves. In this case Green's function is obtained from the following equation:

$$\left\{ \frac{1}{c^2} \frac{\partial^2}{\partial t^2} + \Pi^{(TM)} \right\} G^{(TM)}(\mathbf{r}_\parallel, \mathbf{r}'_\parallel, t) = -\delta(\mathbf{r}_\parallel - \mathbf{r}'_\parallel) \delta(t - t') \tag{2.94}$$

Note that since we are considering TM polarized waves, there are no eigenfunctions with 0 angular frequency i.e., there are not any longitudinal waves in this case. The Green's function in the frequency space satisfies the following equation:

$$\left\{ \frac{\omega^2}{c^2} - \Pi^{(TM)} \right\} G^{(TM)}(\mathbf{r}_\parallel, \mathbf{r}'_\parallel, \omega) = -\delta(\mathbf{r}_\parallel - \mathbf{r}'_\parallel) \tag{2.95}$$

The solution to this equation can easily be calculated. Since there are no longitudinal modes we can write down the solution at once by using eqn. 2.90:

$$G^{(TM)}(\mathbf{r}_\parallel, \mathbf{r}_\parallel^{'}, \omega) = \frac{c^2}{\sqrt{2\pi}A} \sum_{\mathbf{k}_\parallel n} \frac{\Xi^{(TM)}_{\mathbf{k}_\parallel n}(\mathbf{r}_\parallel) \otimes \Xi^{(TM)*}_{\mathbf{k}_\parallel n}(\mathbf{r}_\parallel^{'})}{\left(\omega - \omega^{(TM)}_{\mathbf{k}_\parallel n} + i\delta\right) \cdot \left(\omega + \omega^{(TM)}_{\mathbf{k}_\parallel n} + i\delta\right)} \tag{2.96}$$

and the time dependent Green's function can be written as:

$$G^{(TM)}(\mathbf{r}_\parallel, \mathbf{r}_\parallel^{'}, \omega) = -\frac{c^2}{A} \sum_{\mathbf{k}_\parallel n} \Xi^{(TM)}_{\mathbf{k}_\parallel n}(\mathbf{r}_\parallel) \Xi^{(TM)*}_{\mathbf{k}_\parallel n}(\mathbf{r}_\parallel^{'}) \frac{\sin(\omega^{(TM)}_{\mathbf{k}_\parallel n} t)}{\omega^{(TM)}_{\mathbf{k}_\parallel n}} \tag{2.97}$$

2.1.3 Power emitted from an infinitesimal dipole embedded inside a photonic crystal

In the previous section we have found the Green's function. We can now find the solution of Maxwell equations in the presence of a source. In the presence of an external polarization $\mathbf{P}(\mathbf{r}, t)$ Maxwell equations can be written as:

$$\begin{aligned}
\nabla \cdot \{\varepsilon(\mathbf{r})\varepsilon_0 \mathbf{E}(\mathbf{r}, t) + \mathbf{P}(\mathbf{r}, t)\} &= 0 && (2.98)\\
\nabla \cdot \mathbf{H}(\mathbf{r}, t) &= 0 && (2.99)\\
\nabla \times \mathbf{E}(\mathbf{r}, t) &= -\mu_0 \frac{\partial}{\partial t} \mathbf{H}(\mathbf{r}, t) && (2.100)\\
\nabla \times \mathbf{H}(\mathbf{r}, t) &= \frac{\partial}{\partial t} \{\varepsilon(\mathbf{r})\varepsilon_0 \mathbf{E}(\mathbf{r}, t) + \mathbf{P}(\mathbf{r}, t)\} && (2.101)
\end{aligned}$$

To solve these equations in terms of the Green's function we have derived in the previous section, we need to put these equations in a form containing the operator Π. Let us first eliminate $\mathbf{H}$ from the above Maxwell equations:

$$\nabla \times \nabla \times \mathbf{E}(\mathbf{r}, t) = -\mu_0 \frac{\partial}{\partial t} \nabla \times \mathbf{H}(\mathbf{r}, t)$$

$$\nabla \times (\nabla \times \mathbf{E}(\mathbf{r},t)) = -\mu_0 \frac{\partial^2}{\partial t^2} \{\varepsilon(\mathbf{r})\varepsilon_0 \mathbf{E}(\mathbf{r},t) + \mathbf{P}(\mathbf{r},t)\}$$

$$-\left\{ \frac{1}{\sqrt{\varepsilon(\mathbf{r})}c^2} \frac{\partial^2}{\partial t^2}\mathbf{E}(\mathbf{r},t) + \frac{1}{\sqrt{\varepsilon(\mathbf{r})}} \nabla \times (\nabla \times \mathbf{E}(\mathbf{r},t)) \right\} = \frac{1}{c^2 \varepsilon_0 \sqrt{\varepsilon(\mathbf{r})}} \frac{\partial^2}{\partial t^2}\mathbf{P}(\mathbf{r},t) \tag{2.102}$$

Notice that

$$\frac{1}{\sqrt{\varepsilon(\mathbf{r})}} \nabla \times (\nabla \times \mathbf{E}(\mathbf{r},t)) = \frac{1}{\sqrt{\varepsilon(\mathbf{r})}} \nabla \times \left(\nabla \times \frac{1}{\sqrt{\varepsilon(\mathbf{r})}} \mathbf{\Xi}(\mathbf{r},t) \right) = \Pi \mathbf{\Xi}(\mathbf{r},t)$$

then eqn. 2.102 can be written as:

$$-\left\{ \frac{1}{c^2} \frac{\partial^2}{\partial t^2} \mathbf{\Xi}(\mathbf{r},t) + \Pi \mathbf{\Xi}(\mathbf{r},t) \right\} = \frac{1}{c^2 \varepsilon_0 \sqrt{\varepsilon(\mathbf{r})}} \frac{\partial^2}{\partial t^2} \mathbf{P}(\mathbf{r},t) \tag{2.103}$$

The solution to this equation can written via the Green's function, eqn. 2.91,

$$\mathbf{E}(\mathbf{r},t) = \frac{1}{\sqrt{\varepsilon(\mathbf{r})}} \int_V dV \int_{-\infty}^{\infty} dt' \overleftrightarrow{G}(\mathbf{r},\mathbf{r}',t-t') \frac{1}{c^2 \varepsilon_0 \sqrt{\varepsilon(\mathbf{r}')}} \frac{\partial^2}{\partial t'^2} \mathbf{P}(\mathbf{r}',t') \tag{2.104}$$

Let us insert the Green's function, eqn. 2.91, to eqn. 2.104

$$\mathbf{E}(\mathbf{r},t) = -\frac{1}{\varepsilon_0 V \sqrt{\varepsilon(\mathbf{r})}} \sum_{\mathbf{k}n} \int_V dV \int_{-\infty}^{t} dt' \{ \mathbf{\Xi}_{\mathbf{k}n}^{(T)}(\mathbf{r}) \otimes \mathbf{\Xi}_{\mathbf{k}n}^{(T)*}(\mathbf{r}') \frac{\sin(\omega_{\mathbf{k}n}^{(T)} \left[t-t'\right])}{\omega_{\mathbf{k}n}^{(T)}}$$

$$+ \left[t-t'\right] \mathbf{\Xi}_{\mathbf{k}n}^{(L)}(\mathbf{r}) \otimes \mathbf{\Xi}_{\mathbf{k}n}^{(L)*}(\mathbf{r}') \} \frac{1}{\sqrt{\varepsilon(\mathbf{r}')}} \frac{\partial^2}{\partial t'^2} \mathbf{P}(\mathbf{r}',t') \tag{2.105}$$

In the above equation external polarization is introduced adiabatically to the system. Using integration by parts we obtain:

$$\mathbf{E}(\mathbf{r},t) = -\frac{1}{\varepsilon_0 V\sqrt{\varepsilon(\mathbf{r})}}\sum_{\mathbf{k}n}\int_V dV\int_{-\infty}^{t} dt^{'}\{\mathbf{\Xi}_{\mathbf{k}n}^{(T)}(\mathbf{r})\otimes\mathbf{\Xi}_{\mathbf{k}n}^{(T)*}(\mathbf{r}^{'})\cos(\omega_{\mathbf{k}n}^{(T)}\left[t-t^{'}\right]) + \mathbf{\Xi}_{\mathbf{k}n}^{(L)}(\mathbf{r})\otimes\mathbf{\Xi}_{\mathbf{k}n}^{(L)*}(\mathbf{r}^{'})\}\frac{1}{\sqrt{\varepsilon(\mathbf{r}^{'})}}\frac{\partial}{\partial t^{'}}\mathbf{P}(\mathbf{r}^{'},t^{'}) \tag{2.106}$$

Using integration by parts once more we obtain:

$$\mathbf{E}(\mathbf{r},t) = -\frac{1}{\varepsilon_0 V\sqrt{\varepsilon(\mathbf{r})}}\sum_{\mathbf{k}n}\int_V dV\{\mathbf{\Xi}_{\mathbf{k}n}^{(T)}(\mathbf{r})\otimes\mathbf{\Xi}_{\mathbf{k}n}^{(T)*}(\mathbf{r}^{'})+\mathbf{\Xi}_{\mathbf{k}n}^{(L)}(\mathbf{r})\otimes\mathbf{\Xi}_{\mathbf{k}n}^{(L)*}(\mathbf{r}^{'})\}\frac{1}{\sqrt{\varepsilon(\mathbf{r}^{'})}}\mathbf{P}(\mathbf{r}^{'},t^{'}) + \frac{1}{\varepsilon_0 V\sqrt{\varepsilon(\mathbf{r})}}\sum_{\mathbf{k}n}\int_V dV\int_{-\infty}^{t} dt^{'}\left\{\omega_{\mathbf{k}n}^{(T)}\sin(\omega_{\mathbf{k}n}^{(T)}\left[t-t^{'}\right])\mathbf{\Xi}_{\mathbf{k}n}^{(T)}(\mathbf{r})\otimes\mathbf{\Xi}_{\mathbf{k}n}^{(T)*}(\mathbf{r}^{'})\right\}\frac{1}{\sqrt{\varepsilon(\mathbf{r}^{'})}}\mathbf{P}(\mathbf{r}^{'},t^{'}) \tag{2.107}$$

This equation can be simplified further by using eqn. 2.83:

$$\mathbf{E}(\mathbf{r},t) = -\frac{\mathbf{P}(\mathbf{r},t)}{\varepsilon_0\varepsilon(\mathbf{r})} + \frac{1}{\varepsilon_0 V\sqrt{\varepsilon(\mathbf{r})}}\sum_{\mathbf{k}n}\mathbf{\Xi}_{\mathbf{k}n}^{(T)}(\mathbf{r})\times \int_V dV\int_{-\infty}^{t}\frac{\mathbf{\Xi}_{\mathbf{k}n}^{(T)*}(\mathbf{r}^{'})\cdot\mathbf{P}(\mathbf{r}^{'},t^{'})}{\sqrt{\varepsilon(\mathbf{r}^{'})}}\omega_{\mathbf{k}n}^{(T)}\sin(\omega_{\mathbf{k}n}^{(T)}\left[t-t^{'}\right])dt^{'} \tag{2.108}$$

In terms of electric field:

$$\mathbf{E}(\mathbf{r},t) = -\frac{\mathbf{P}(\mathbf{r},t)}{\varepsilon_0\varepsilon(\mathbf{r})}+\frac{1}{\varepsilon_0 V}\sum_{\mathbf{k}n}\mathbf{E}_{\mathbf{k}n}^{(T)}(\mathbf{r})\int_V dV\int_{-\infty}^{t}\mathbf{E}_{\mathbf{k}n}^{(T)*}(\mathbf{r}^{'})\cdot\mathbf{P}(\mathbf{r}^{'},t^{'})\omega_{\mathbf{k}n}^{(T)}\sin(\omega_{\mathbf{k}n}^{(T)}\left[t-t^{'}\right])dt^{'} \tag{2.109}$$

We can now the discuss the dipole radiation. For the external polarization we consider:

$$\mathbf{P}(\mathbf{r},t) = \mathbf{p}\delta(\mathbf{r}-\mathbf{r}_0)\exp(-i\omega+\delta)t \tag{2.110}$$

$\mathbf{p}$ is the dipole moment and the dipole is located at $\mathbf{r}_0$. Substituting eqn. 2.110 into eqn. 2.109 we obtain:

$$\mathbf{E}(\mathbf{r},t) = -\frac{\mathbf{P}(\mathbf{r},t)}{\varepsilon_0\varepsilon(\mathbf{r})} + \frac{1}{\varepsilon_0 V}\sum_{\mathbf{k}n}\mathbf{E}^{(T)}_{\mathbf{k}n}(\mathbf{r})\int_V dV\int_{-\infty}^{t}$$
$$\mathbf{E}^{(T)*}_{\mathbf{k}n}(\mathbf{r}^{'})\cdot\mathbf{p}\delta\left(\mathbf{r}^{'}-\mathbf{r}_0\right)\exp\{(-i\omega+\delta)t^{'}\}\omega^{(T)}_{\mathbf{k}n}\sin(\omega^{(T)}_{\mathbf{k}n}\left[t-t^{'}\right])dt^{'} \qquad (2.111)$$

performing the integrations following equation is obtained for $\mathbf{E}(\mathbf{r},t)$:

$$\mathbf{E}(\mathbf{r},t) = -\frac{\mathbf{P}(\mathbf{r},t)}{\varepsilon_0\varepsilon(\mathbf{r})} + \frac{\exp(-i\omega t)}{2\varepsilon_0 V}\sum_{\mathbf{k}n}\omega^{(T)}_{\mathbf{k}n}\mathbf{E}^{(T)}_{\mathbf{k}n}(\mathbf{r})\left\{\mathbf{E}^{(T)*}_{\mathbf{k}n}(\mathbf{r}_0)\cdot\mathbf{p}\right\}\times$$
$$\left(\frac{1}{\omega-\omega^{(T)}_{\mathbf{k}n}+i\delta}-\frac{1}{\omega+\omega^{(T)}_{\mathbf{k}n}+i\delta}\right) \qquad (2.112)$$

Magnetic field can be calculated from:

$$\mathbf{H}(\mathbf{r},t) = \frac{1}{i\omega\mu_0}\nabla\times\mathbf{E}(\mathbf{r},t) \qquad (2.113)$$

In the rest of the discussion we will be concerned about the time averaged poynting vector:

$$\overline{\mathbf{S}(\mathbf{r},t)} = \overline{\{\mathbf{E}(\mathbf{r},t)+\mathbf{E}^{*}(\mathbf{r},t)\}\times\{\mathbf{H}(\mathbf{r},t)+\mathbf{H}^{*}(\mathbf{r},t)\}} \qquad (2.114)$$

The power emitted in unit time by the dipole is the surface integral of the normal component of the Poynting vector. The surface integral can be converted to a volume integral by the identity:

$$\int_A d\mathbf{A}\cdot\mathbf{A}(\mathbf{r}) = \int_V \nabla_{\mathbf{r}}\cdot\mathbf{A}(\mathbf{r})dV \qquad (2.115)$$

Hence, we will calculate $\overline{\nabla_{\mathbf{r}}\cdot\mathbf{S}(\mathbf{r},t)}$. By the help of Maxwell eqns. 2.98 and eqn. 2.113 we obtain:

$$\begin{aligned}\overline{\nabla_{\mathbf{r}} \cdot \mathbf{S}(\mathbf{r},t)} &= \mathbf{H}(\mathbf{r},t) \cdot \{\nabla \times \mathbf{E}(\mathbf{r},t)\} - \mathbf{E}(\mathbf{r},t) \cdot \{\nabla \times \mathbf{H}^*(\mathbf{r},t)\} \\ &+\mathbf{H}(\mathbf{r},t) \cdot \{\nabla \times \mathbf{E}^*(\mathbf{r},t)\} - \mathbf{E}^*(\mathbf{r},t) \cdot \{\nabla \times \mathbf{H}(\mathbf{r},t)\} \\ &= i\omega \left\{\mathbf{E}^*(\mathbf{r},t) \cdot \mathbf{P}(\mathbf{r},t) - \mathbf{E}(\mathbf{r},t) \cdot \mathbf{P}^*(\mathbf{r},t)\right\} \end{aligned} \tag{2.116}$$

This equation can be evaluated by substituting eqn. 2.112 and by the help of the following identity:

$$\lim_{\overrightarrow{\delta \to 0}} \frac{1}{\omega - \omega_{\mathbf{k}n}^{(T)} \pm i\delta} = \mathrm{Pr}\,. \frac{1}{\omega - \omega_{\mathbf{k}n}^{(T)}} \mp i\pi\delta(\omega - \omega_{\mathbf{k}n}^{(T)}) \tag{2.117}$$

The result is:

$$\begin{aligned}\overline{\nabla_{\mathbf{r}} \cdot \mathbf{S}(\mathbf{r},t)} &= \frac{\pi\omega^2}{\varepsilon_0 V} \delta\left(\mathbf{r} - \mathbf{r}_0\right) \sum_{\mathbf{k}n} \left|\mathbf{p} \cdot \mathbf{E}_{\mathbf{k}n}^{(T)*}(\mathbf{r}_0)\right|^2 \delta(\omega - \omega_{\mathbf{k}n}^{(T)}) \\ &= \frac{\pi\omega^2}{\varepsilon_0 V} \delta\left(\mathbf{r} - \mathbf{r}_0\right) \sum_{\mathbf{k}n} \left|\mathbf{p} \cdot \mathbf{E}_{\mathbf{k}n}^{(T)*}(\mathbf{r}_0)\right|^2 \frac{\delta(\mathbf{k} - \mathbf{k}n)}{\left|\frac{\partial}{\partial \mathbf{k}} \omega(\mathbf{k})\right|_{\mathbf{k}n}} \end{aligned} \tag{2.118}$$

since

$$|v_g| = \left|\frac{\partial}{\partial \mathbf{k}} \omega(\mathbf{k})\right|_{\mathbf{k}n}$$

equation 2.118 can be written in terms of the group velocity v_g as:

$$\overline{\nabla_{\mathbf{r}} \cdot \mathbf{S}(\mathbf{r},t)} = \frac{\pi\omega^2}{\varepsilon_0 V} \delta\left(\mathbf{r} - \mathbf{r}_0\right) \sum_{\mathbf{k}n} \left|\mathbf{p} \cdot \mathbf{E}_{\mathbf{k}n}^{(T)*}(\mathbf{r}_0)\right|^2 \frac{\delta(\mathbf{k} - \mathbf{k}n)}{|v_g|} \tag{2.119}$$

Following remarks will be of help when we discuss the emission of radiation from a source embedded inside a photonic crystal.

- Due to the term $\left|\mathbf{p} \cdot \mathbf{E}_{\mathbf{k}n}^{(T)*}(\mathbf{r}_0)\right|^2$ the emission of radiation depends on the electric field intensity of the modes at the source location. Also the dependence on the polarization of the source is evident.
- From eqn. 2.119 we observe that the emitted power is inversely proportional to the group velocity of the modes.

2.1.4 Group velocity calculation

In the previous section when we calculated the normal component of the Poynting vector we found out that the emitted power is inversely proportional to the magnitude of the group velocity. Hence, it essential to have a knowledge of the group velocity when we deal with the emission of radiation problem. In this section we will explain the $\mathbf{k} \cdot \mathbf{p}$ perturbation method.

This method is well-known in the solid state theory. First, we will derive the differential equation for the lattice periodic function $\mathbf{u}_{\mathbf{k}n}(\mathbf{r})$ appearing in the Bloch form. Then, we will consider the differential equation satisfied for the lattice periodic function $\mathbf{u}_{\mathbf{k}+\triangle\mathbf{p}n}(\mathbf{r})$ where $\triangle p$ is an infinitesimal wave vector. We will treat the term arising by the introduction of $\triangle p$ as a small perturbation term.

Let us try to find the differential equation satisfied by $\mathbf{u}_{\mathbf{k}n}(\mathbf{r})$. The differential equation satisfied by $\mathbf{E}_{\mathbf{k}n}(\mathbf{r})$ is given by eqn. 2.20 and the Bloch form for $\mathbf{E}_{\mathbf{k}n}(\mathbf{r})$ is given in eqn. 2.24. Inserting eqn. 2.24 into eqn. 2.20 and using the following identity,

$$\nabla \times (\varphi \mathbf{a}) = \nabla\varphi \times \mathbf{a} + \varphi \nabla \times \mathbf{a} \tag{2.120}$$

we obtain:

$$\begin{aligned}\frac{\omega^2}{c^2}\epsilon(\mathbf{r})\mathbf{u}_{\mathbf{k}n}(\mathbf{r}) = &-\mathbf{k}\cdot(\mathbf{k}\cdot\mathbf{u}_{\mathbf{k}n}(\mathbf{r})) + \mathbf{u}_{\mathbf{k}n}(\mathbf{r})k^2 + i\mathbf{k}\cdot(\nabla\mathbf{u}_{\mathbf{k}n}(\mathbf{r})) \\ &+\nabla(\mathbf{k}\cdot\mathbf{u}_{\mathbf{k}n}(\mathbf{r})) + \nabla(\nabla\mathbf{u}_{\mathbf{k}n}(\mathbf{r})) - \nabla^2\mathbf{u}_{\mathbf{k}n}(\mathbf{r})\end{aligned} \tag{2.121}$$

For a $2D$ photonic crystal eqn. 2.121 can be simplified by the fact that $\mathbf{k}$ is orthogonal to $\mathbf{u}_{\mathbf{k}n}(\mathbf{r})$ for TM polarized waves. And finally in $2D$ case $u_{\mathbf{k}n}(\mathbf{r})$ satisfies the following differential equation:

$$\left\{\nabla_{xy}^2 + 2i\mathbf{k}_\parallel\cdot\nabla_{xy} - k_\parallel^2\right\} u_{z,\mathbf{k}_\parallel n}(\mathbf{r}_\parallel) + \frac{\omega_{z,\mathbf{k}_\parallel n}^2}{c^2}\epsilon(\mathbf{r}_\parallel)u_{z,\mathbf{k}_\parallel n}(\mathbf{r}_\parallel) = 0 \tag{2.122}$$

And the differential equation satisfied by $\mathbf{u}_{\mathbf{k}+\triangle\mathbf{p}n}(\mathbf{r})$ can be written as:

$$\left\{\nabla_{xy}^2 + 2i\mathbf{k}_\parallel\cdot\nabla_{xy} - k_\parallel^2\right\} u_{z,\mathbf{k}_\parallel+\triangle\mathbf{p}n}(\mathbf{r}_\parallel) - \left[2\triangle\mathbf{p}\cdot\left\{-i\nabla + \mathbf{k}_\parallel\right\} + |\triangle\mathbf{p}|^2\right] u_{z,\mathbf{k}_\parallel+\triangle\mathbf{p}n}(\mathbf{r}_\parallel)$$
$$+\frac{\omega_{z,\mathbf{k}_\parallel+\triangle\mathbf{p}n}^2}{c^2}\epsilon(\mathbf{r}_\parallel)u_{z,\mathbf{k}_\parallel+\triangle\mathbf{p}n}(\mathbf{r}_\parallel) = 0 \tag{2.123}$$

Since $\triangle\mathbf{p}$ is infinitesimally small second term,

$$\left[2\triangle\mathbf{p}\cdot\left\{-i\nabla + \mathbf{k}_\parallel\right\} + |\triangle\mathbf{p}|^2\right] \tag{2.124}$$

can be treated as a perturbation term and the methods of the perturbation theory can be applied to calculate the eigenvalues of eqn. 2.123. Hence, eigenvalues of eqn. 2.123 can be written as a perturbation series in $\triangle\mathbf{p}$. Moreover, if we expand the eigenvalues of eqn. 2.123, $\omega_{z,\mathbf{k}_\parallel+\triangle\mathbf{p}n}^2$, in a Taylor series in $\triangle\mathbf{p}$ we obtain:

$$\omega_{z,\mathbf{k}_\parallel+\triangle\mathbf{p}n} = \omega_{z,\mathbf{k}_\parallel} + \triangle\mathbf{p}.\nabla_k\omega_{z,\mathbf{k}_\parallel} + ... \tag{2.125}$$

Remember that $\nabla_k\omega_{z,\mathbf{k}_\parallel}$ is the group velocity of the modes. Now we may match the coefficients of the powers of $\triangle\mathbf{p}$ between the terms in the Taylor series expansion and the terms in perturbation expansion. The equality of the terms is implied by the uniqueness of the power series expansion. The final result can be written in terms of the eigenfunctions of the Maxwell equations as:

$$\mathbf{v}_{g,\mathbf{k}_\parallel n} = \frac{c^2}{\omega_{z,\mathbf{k}_\parallel n}} < E_{z,\mathbf{k}_\parallel n}(\mathbf{r}_\parallel) \mid -i\nabla \mid E_{z,\mathbf{k}_\parallel n}(\mathbf{r}_\parallel) > \tag{2.126}$$

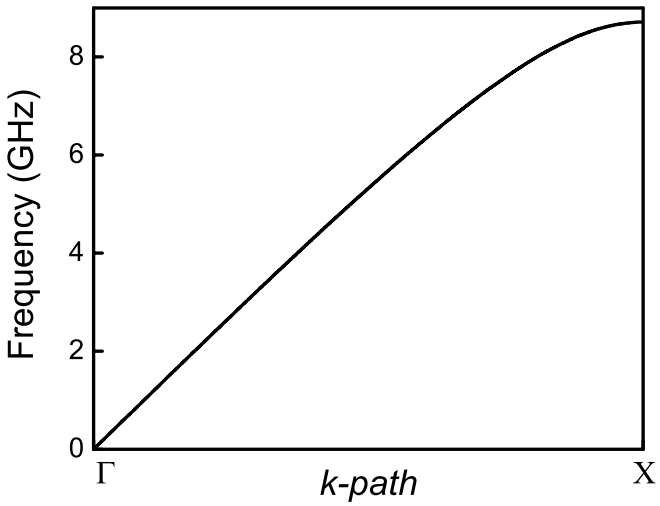

Figure 2.6: First TM polarized band along $\Gamma - X$ direction.

Hence, once the eigenfunction and eigenvalue for a particular $\mathbf{k}$ and n has been calculated, group velocity can be calculated easily.

We will now present the results of the group velocity calculations for the particular case that we have discussed in the first section. The crystal consist of a square array of alumina rods whose radius is 1.575 mm. The lattice constant is 11 mm and the dielectric constant of the rods is 9.61. The band structure along $\Gamma - X$ is given in Fig. 2.6 and the corresponding group velocity for the first band is presented in Fig. 2.7

From Fig. 2.7 we observe that the group velocity of the mode at X point is vanishingly small for a perfect, infinite crystal. We shall note that since the lower edge of the first band gap is not at the X point, there are modes in other directions and these modes also have the same frequency of the mode that is at X point. We will discuss this point when we consider the radiation problem of a source embedded inside a photonic crystal.

Let us now check the group velocity for the second band along $\Gamma - X$ direction. The band structure for the second TM polarized band along $\Gamma - X$ is given in

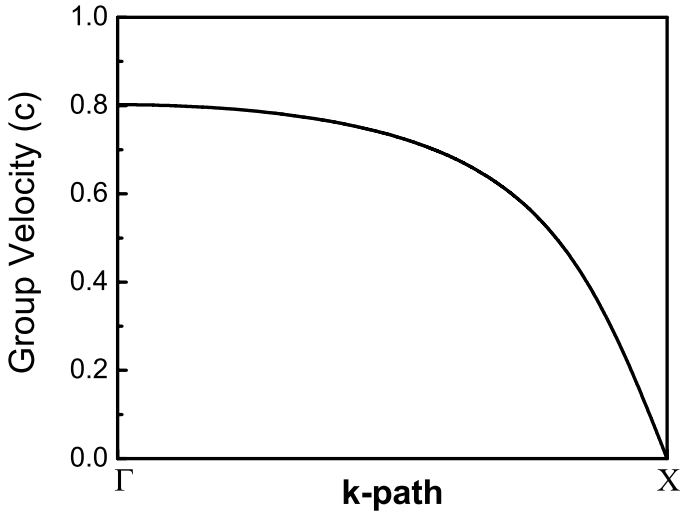

Figure 2.7: Group velocity of the modes of the first TM polarized band along $\Gamma - X$ direction.

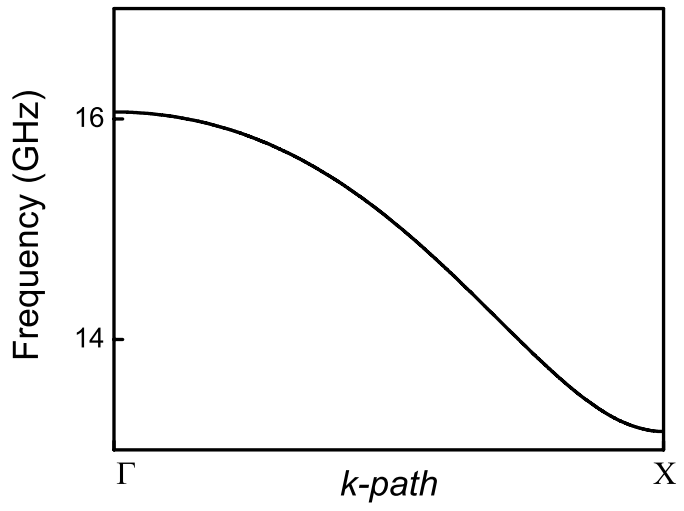

Figure 2.8: Second TM polarized band along $\Gamma - X$ direction.

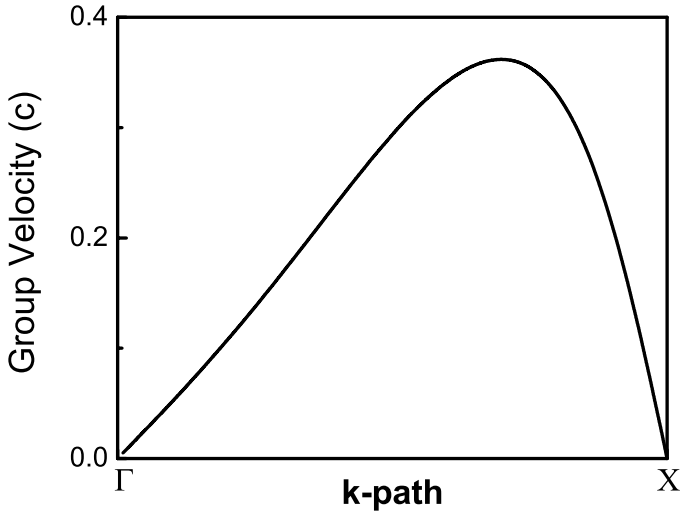

Figure 2.9: Group velocity of the modes of the second TM polarized band along $\Gamma - X$ direction.

Fig. 2.8 and the corresponding group velocities is presented in Fig. 2.9

We also observe from Fig. 2.9 that the group velocity is vanishingly small at X point for the second band. Moreover, from Fig. 2.3 we observe that the upper band edge of the first band gap is X point. Hence, there are no other modes with the same frequency. This point will be of use later in the discussion.

2.2 The FDTD method

In this section we will discuss the FDTD method without going into too much detail. We will present some transmission results for the photonic crystal we discussed in the previous sections.

FDTD method is a direct space-time approach. In this method an initial field is sent to the domain of calculation and its temporal and spatial evolution is analyzed [31].

To the first order, the derivative of a function of x can be approximated as:

$$\frac{d}{dx}f(x) \approx \frac{f(x+\triangle/2 - f(x-\triangle/2)}{\triangle} \tag{2.127}$$

In this equation $\triangle$ is assumed to be small. Maxwell equations relate the components of the electric field and magnetic field. These components are functions of the spatial coordinates and time. Let us consider the Maxwell curl equations. Written in component form we have six scalar equations. Particularly let us consider two of them:

$$\frac{\partial}{\partial t}H_x = -\frac{1}{\mu}\left\{\frac{\partial}{\partial z}E_y - \frac{\partial}{\partial y}E_z\right\} \tag{2.128}$$

$$\frac{\partial}{\partial t}E_y = -\frac{1}{\varepsilon}\left\{\frac{\partial}{\partial z}H_x - \frac{\partial}{\partial x}H_z\right\} \tag{2.129}$$

Time and spatial derivatives appearing in these equations can be approximated by the help of eqn. 2.127. But in order to achieve useful results these derivatives must be approximated in a special way. The algorithm due to Yee [32] is the most used one in approximating the eqn. 2.128. The algorithm is explained in Fig. 2.10.

In the Yee algorithm electric and magnetic field components are calculated at points shown in Fig. 2.10. The grid points are spaced $\triangle x$, $\triangle y$, and $\triangle z$ apart. The electric and the magnetic field components are then interlaced in all three spatial dimensions. On the other hand time is divided into steps of $\triangle t$. Electric field components are then computed at times $t = n \triangle t$ whereas the magnetic field components are calculated at times $t = (n+1/2)\triangle t$. This algorithm is also known as the leap-frog algorithm.

Let us write down the results for two particular components of the electric field and magnetic field. x component of the magnetic field can be written as:

$$H^{n+1/2}_{x(i,j,k)} = H^{n-1/2}_{x(i,j,k)} + \frac{\triangle t}{\mu \triangle z}\left\{E^n_{y(i,j,k)} - E^n_{y(i,j,k-1)}\right\} - \frac{\triangle t}{\mu \triangle y}\left\{E^n_{z(i,j,k)} - E^n_{z(i,j,k-1)}\right\} \tag{2.130}$$

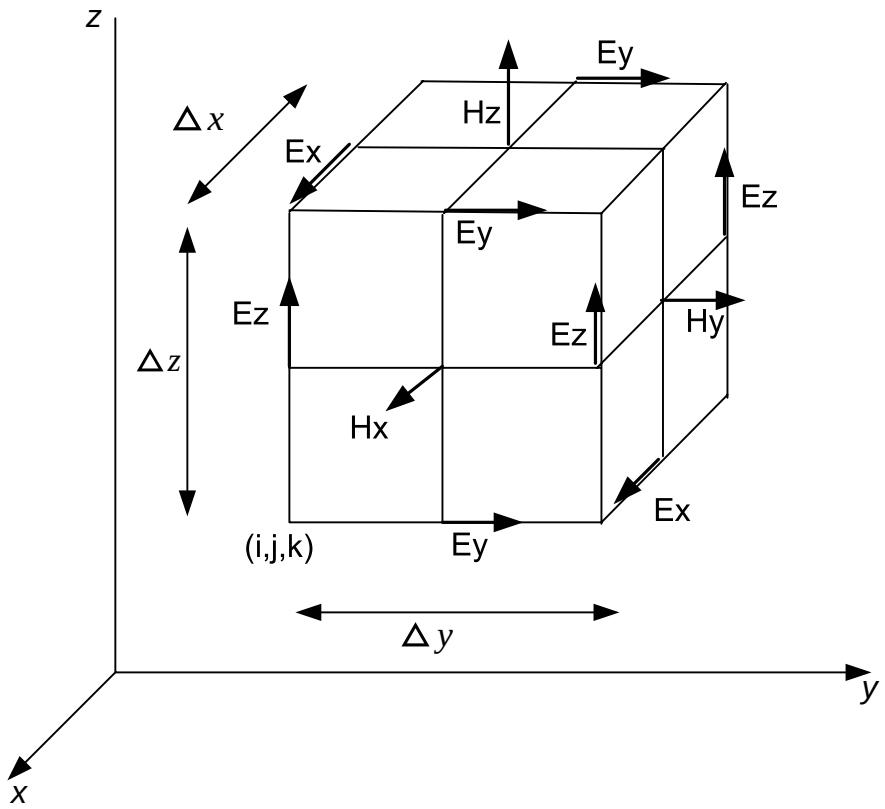

Figure 2.10: The grid on which the Yee algorithm is defined. It is known as the Yee cell. Magnetic field is calculated at points half-shifted with respects to the points at which the electric field is calculated.

and the x component of the electric field can be written as:

$$E^{n+1}_{x(i,j,k)} = E^{n}_{x(i,j,k)} + \frac{\triangle t}{\varepsilon \triangle y}\left\{H^{n+1/2}_{y(i,j+1,k)} - H^{n+1/2}_{y(i,j,k)}\right\} - \frac{\triangle t}{\varepsilon \triangle z}\left\{H^{n+1/2}_{z(i,j,k+1)} - H^{n+1/2}_{z(i,j,k)}\right\} \tag{2.131}$$

Looking at the form of eqns. 2.130 and 2.131, we observe that once we know the electric field and magnetic field at some point in time at all grid points, we can use the above equations to find the field components at later times. Hence, we need to introduce an initial excitation into the domain of calculation. Usually, if one needs to calculate the spectral response, it is useful to introduce a Gaussian pulse that is a function of time.

For the boundary conditions, we usually use a special boundary condition in our calculations. These boundary conditions are known as the perfectly matched layer (PML) boundary conditions. PML boundary conditions simulate an infinitely large open space around the computation domain.

We used FDTD method to calculate the transmission and angular distribution of power.

2.3 Reflection and refraction

In this section we will examine an important problem i.e., reflection and refraction of monochromatic plane waves from a photonic crystal. Before discussing the reflection and refraction from photonic crystals let us discuss the following problem: plane monochromatic waves incident on a uniform medium.

Incident, reflected, and refracted waves can be written as:

$$\mathbf{E}_i = \mathbf{E}_0 \exp(i\{\mathbf{k}_i \cdot \mathbf{r} - \omega_i t\}) \tag{2.132}$$

$$\mathbf{E}_r = \mathbf{E}_{0r} \exp(i\{\mathbf{k}_r \cdot \mathbf{r} - \omega_r t\}) \tag{2.133}$$

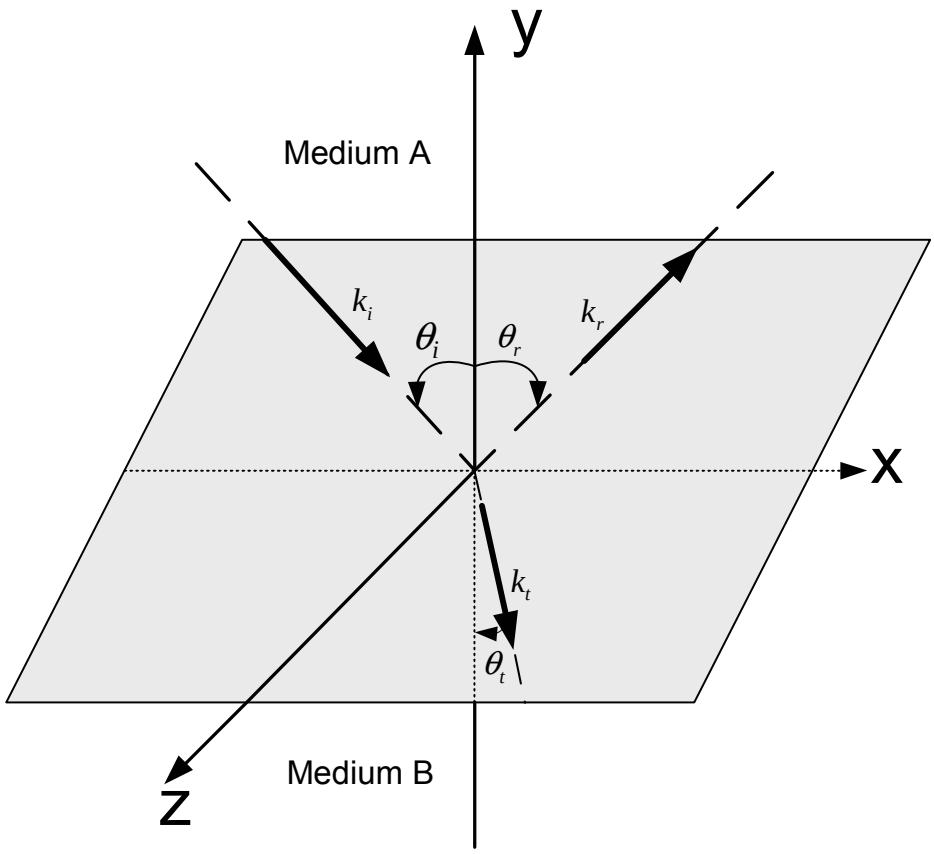

Figure 2.11: Plane monochromatic waves with wave vector $\mathbf{k}_i$ are incident on medium B from medium A. The reflected and refracted waves have wave vectors $\mathbf{k}_r$ and $\mathbf{k}_t$

$$\mathbf{E}_t = \mathbf{E}_{0t} \exp(i\{\mathbf{k}_t \cdot \mathbf{r} - \omega_t t\}) \tag{2.134}$$

The boundary conditions are:

$$\mathbf{n}_i \times \mathbf{E}_i + \mathbf{n}_i \times \mathbf{E}_r = \mathbf{n}_t \times \mathbf{E}_t \tag{2.135}$$

$$\varepsilon_i \left(\mathbf{n}_i \cdot \mathbf{E}_i + \mathbf{n}_i \cdot \mathbf{E}_r\right) = \varepsilon_t \mathbf{n}_t \cdot \mathbf{E}_t \tag{2.136}$$

Equation 2.135 states that the tangential components of the electric on either sides of the interface are conserved at all times at $y = 0$, Fig. 2.11, i.e.,

$$\{\mathbf{k}_i \cdot \mathbf{r} - \omega_i t\} = \{\mathbf{k}_r \cdot \mathbf{r} - \omega_r t\} = \{\mathbf{k}_t \cdot \mathbf{r} - \omega_t t\} \tag{2.137}$$

This equation needs to be satisfied at all times, which means that:

$$\omega_i = \omega_r = \omega_t \tag{2.138}$$

Equality of angular frequencies is the statement of the conservation of energy.

Equation 2.137 needs to be satisfied at all $\mathbf{r}_{|y=0}$, which is equivalent to conservation of the tangential component of the wave vector on either sides of the interface. We can rephrase the conservation of the tangential component of the wave vector in a slightly different way. Since the system is invariant under translations in $x - y$ plane, the momentum component parallel to $x - y$ plane has to be conserved.

Let us put these observations into the language of equal frequency contour analysis. For a uniform medium we have the following dispersion relation:

$$|\mathbf{k}| = \sqrt{\left(k_x^2 + k_y^2 + k_z^2\right)} = n\frac{\omega}{c} \tag{2.139}$$

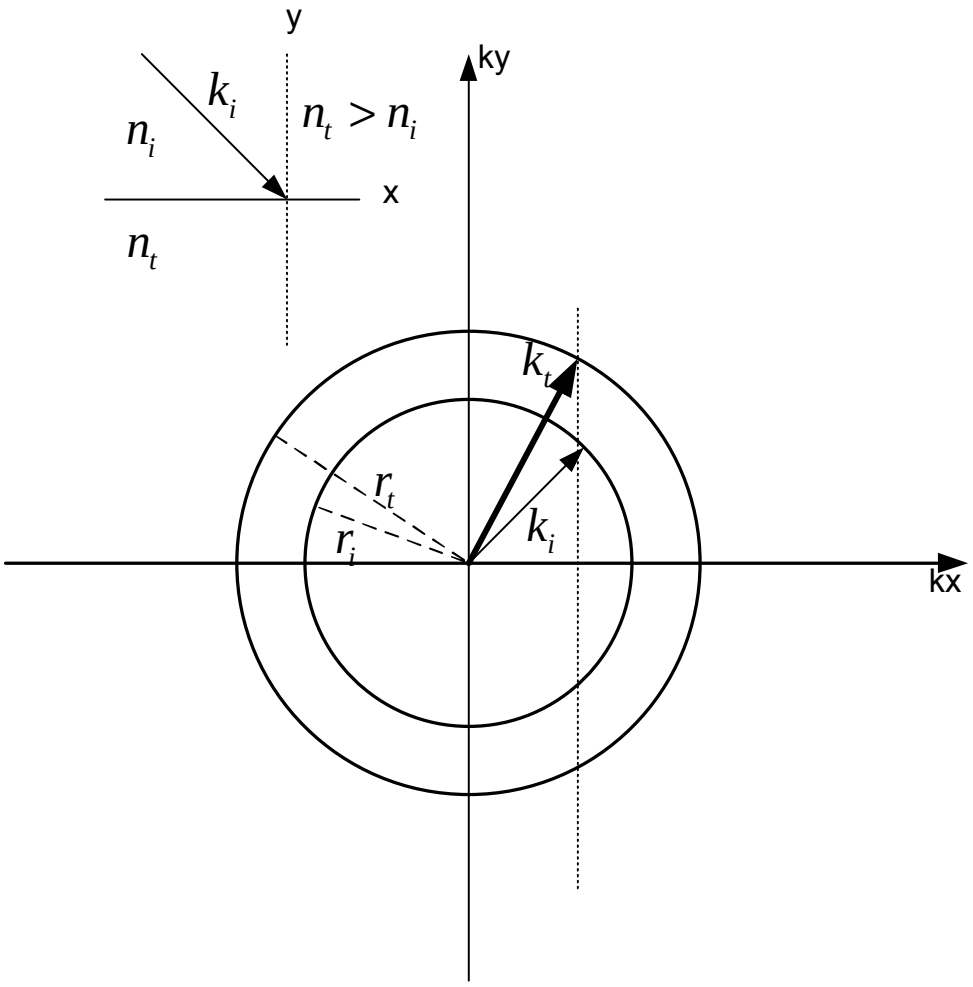

Figure 2.12: Equal frequency analysis for two uniform medium. Radiuses of the circles are determined by the index of refraction of the mediums and the frequency of the incident plane wave. $\mathbf{k}_t$ is determined by the condition of conservation of the tangential component of the wave vector.

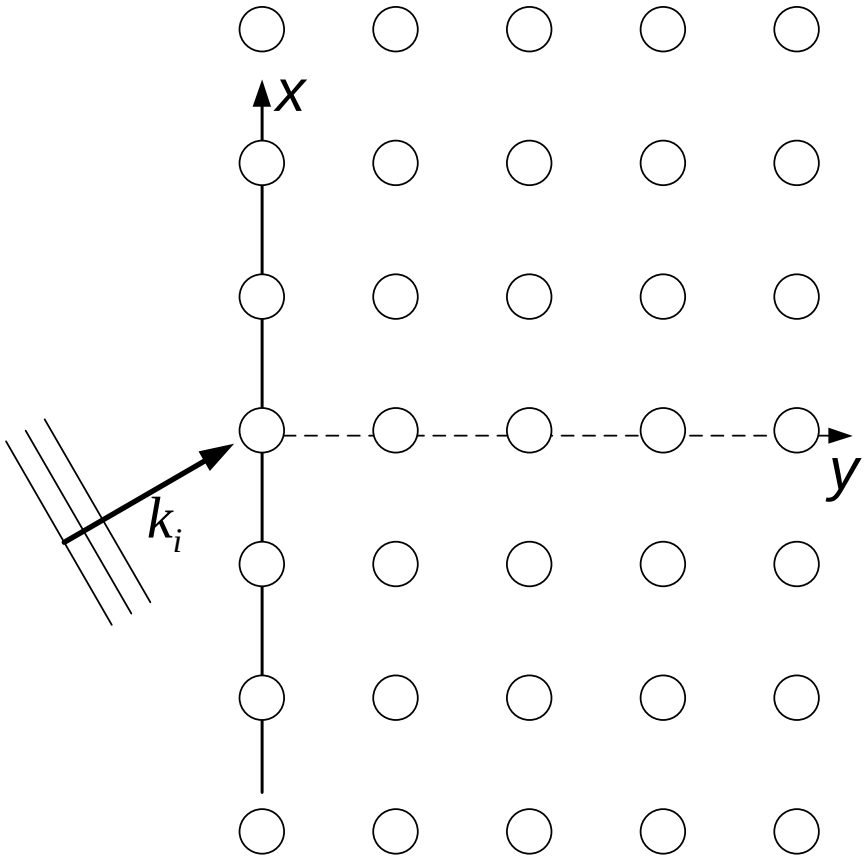

Figure 2.13: Plane monochromatic waves are incident on the photonic crystal. Upon refraction tangential component of the wave vector $\mathbf{k}_{ix}$ is conserved.

This defines a sphere in wave vector space with radius $n\frac{\omega}{c}$. For the sake of simplicity we will consider a two dimensional system where eqn. 2.139 defines a circle. The above observations can be put into a simple equal frequency diagram: we draw two circles with radiuses of $n_i\frac{\omega}{c}$ and $n_t\frac{\omega}{c}$, where n_i is the index of refraction of medium A and n_t is the index of refraction of medium B. This is equivalent to conservation of energy. To determine the wave vector of the refracted wave we need to use the conservation of the tangential component of the momentum, Fig. 2.12.

Let us now analyze the same problem for plane monochromatic waves incident on a photonic crystal. In section 2.1.1 we saw that the eigenvalues of the Maxwell equations for a photonic crystal are periodic in the wave vector space, i.e.,

$$\omega_{n,\mathbf{k}+\mathbf{G}} = \omega_{n,\mathbf{k}} \tag{2.140}$$

We need to take into account the periodicity of the the angular frequency in our equal frequency contour analysis. If plane monochromatic waves with angular frequency ω are incident on the photonic crystal with wave vector $\mathbf{k}$, Fig. 2.13, the conservation of the tangential component of the wave vector and the conservation of energy implies that:

$$\mathbf{k}_{t\|} = \mathbf{k}_{i\|} + \mathbf{G}_{\|} \tag{2.141}$$

For the sake of simplicity let us assume that for a particular angular frequency ω the dispersion relation for a photonic crystal defines a circle with radius γ in the first brillouin zone. In the wave vector space this is equivalent to circles with radius γ centered at the reciprocal lattice points. Determination of the wave vectors of the refracted waves is outlined in Fig. 2.14. The allowed wave vectors are $\mathbf{k}_{t1}$, $\mathbf{k}_{t2} = \mathbf{k}_{t1} + \frac{2\pi}{a}$ ..., i.e., $\mathbf{k}_{tn} = \mathbf{k}_{t1} + n\frac{2\pi}{a}$. The wave vectors denoted by $\mathbf{k}_{-nt}$ are not allowed since these are backward propagating waves.

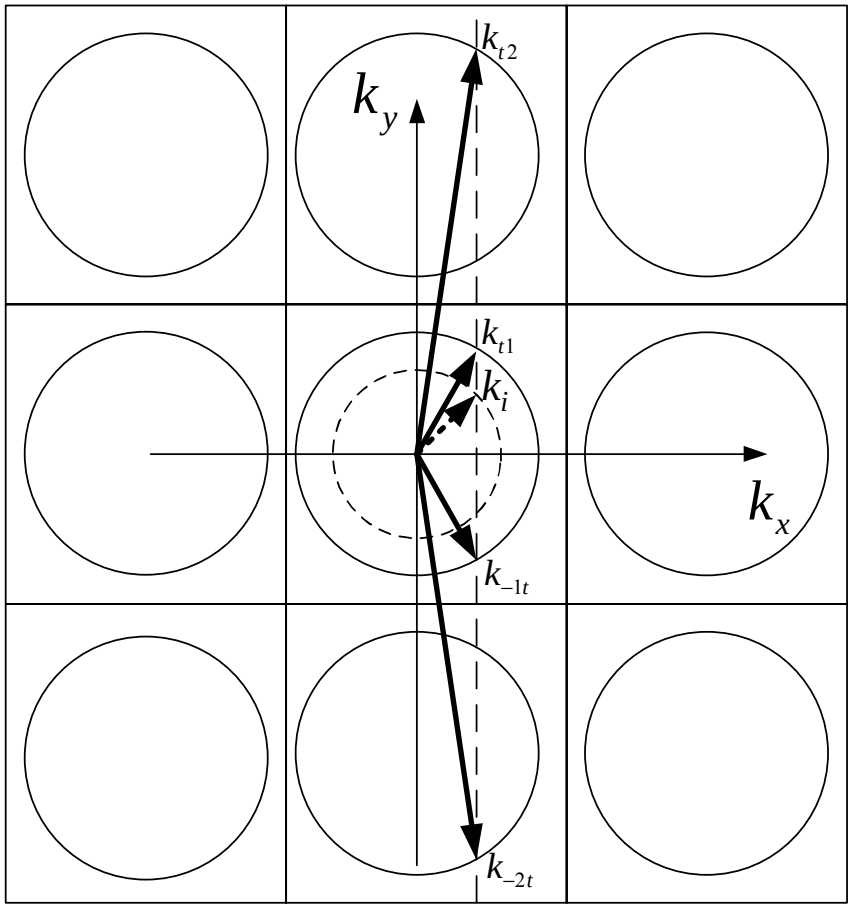

Figure 2.14: Equal frequency analysis for plane monochromatic waves incident on the photonic crystal. Equal frequency contours in wave vector space for the particular ω is circular in this case. The wave vectors of the refracted waves are determined by the conservation of frequency and the conservation of the tangential component of the wave vector.

Chapter 3

Enhancement of radiation

3.1 Introduction

As originally proposed by Yablonovitch [14], photonic crystals could be used for the control of spontaneous emission. On the other hand, most of the work devoted to the photonic crystals up to now have focused on the transmission and reflection properties of photonic crystals. However, this provides little insight into how a PC modifies the emission properties of a radiating source. The effect of photonic crystals on the radiation properties of sources have been theoretically investigated by several authors [23, 33, 34, 35, 36]. New phenomena such as photon-atom bound dressed states [35], non-exponential decay of spontaneous emission near the band edge [34], strong inhibition of emission and enormous enhancement of radiation [36] have been reported. These works have revealed that photonic crystals may provide far-reaching control over the spontaneous emission and the radiation dynamics of sources. For instance, spontaneous emission can be enhanced, suppressed or attenuated in all or certain directions by changing the density of modes [36].

Surprisingly, only a few experiments have been reported on the radiation properties of localized sources inside photonic crystals. Preparation of well defined systems is the major problem for such experiments. Some experiments have

been performed to investigate the emission properties of dye molecules embedded inside photonic crystals [37, 38]. These experiments have led to different interpretations and are still subject to discussion [39, 40]. On the other hand, it has been suggested that similar effects such as non-exponential decay rates [41], inhibition of radiation [42], enormous enhancement at the band edges [36] and cavity modes [43] can be observed at longer wavelength scales.

In the previous chapter when we considered the problem of a dipolar source placed inside a photonic crystal we saw that the effect of the photonic crystal on the radiation of a localized source is encapsulated in local density of optical modes (LDOS). For a PC, it has been shown that the Poynting vector, eqn. 2.119, and correspondingly LDOS is proportional to the amplitude of the electric field at the position where the source is located. On the other hand, it is inversely proportional to the group velocity of the mode, $\partial\omega/\partial k$, eqn. 2.119. In this sense, photonic crystals provide enormous control over the radiation of a source, since for a PC it is possible to find positions with high or low electric field amplitude and a mode with low or high group velocity.

In this chapter, we experimentally study the radiation properties of a finite size line source, which we will call hereafter a monopole source, embedded inside a PC. It will be shown that it is possible to enhance the emitted power. Also, radiation properties of a monopole source placed in certain defect structures will be investigated.

3.2 Enhancement of Radiation and Reduced Group Velocities

3.2.1 Experimental Setup

In our experiments, we have used an HP-8510C vector network analyzer. HP-8510C vector network analyzer is capable of measuring both intensity and phase. Details of the experimental setup are summarized in Fig 3.1.

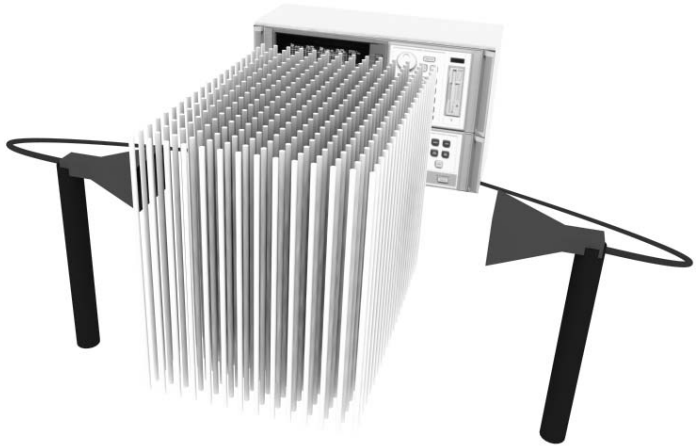

Figure 3.1: Transmission measurement setup. Transmission measurement setup consists of the network analyzer and the transmitter-receiver antennas.

The phase information obtained from the measurement can be used to determine the delay time or the photon lifetime. The photon lifetime is defined as $\tau_p = \partial\varphi/\partial\omega$. Here, φ is the net phase difference between the phase of the EM waves propagating inside the photonic crystal and the phase of the EM waves propagating in free space for a total crystal length of L [44, 45, 46, 47]. Photon lifetime corresponds to the propagation time of the EM waves inside the photonic crystal [48]. Hence, group velocity is inversely proportional to the photon lifetime. Photon lifetime or delay time measurements will be a critical parameter in the following discussion, since the group velocity is inversely proportional to the photon lifetime. The photon lifetime and its certain physical interpretations have been rigorously studied by Ohtaka *et al.* [49, 50, 51, 52]. Ohtaka *et al.* showed that the total optical density of modes is also directly proportional to the photon lifetime [52].

The monopole source is obtained by removing 0.5 cm of the cladding from a coaxial cable and leaving the metal part Fig. 3.2 . The monopole source is then excited by the network analyzer.

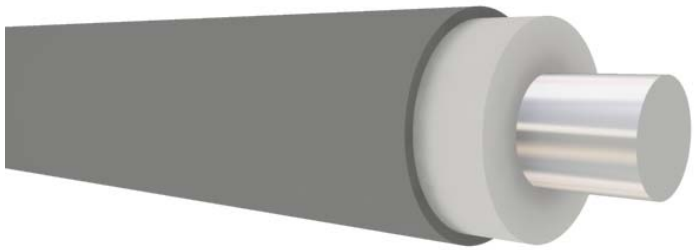

Figure 3.2: The monopole source. The source is obtained by removing the outer jacket of a coaxial cable.

3.2.2 Enhanced Emission from the Monopole at the Band Edges

In chapter 2, we calculated the group velocities for the modes of the first and second band along $\Gamma - X$ direction (Figs. 2.7 and 2.7). We have seen that for a perfect photonic crystal group velocity vanishes near the band edge of the photonic crystal. For a finite PC, the group velocities of the modes at the band edges do not vanish but still the group velocities for these modes are expected to be small [53, 54, 55] and correspondingly, the photon lifetimes are expected to be high. Hence, it follows that LDOS is high at the band edge modes as LDOS is inversely proportional to the group velocity.

The PC used in the experiments is a 25×25 square array of cylindrical alumina rods whose radius is 1.55 mm and dielectric constant is 9.61. The separation between the center of rods along lattice vectors is $a = 11$ mm. The structure that we have used in our experiments has a filling fraction of 0.062. This structure is similar to the photonic crystal that we used as an example in chapter 2. The

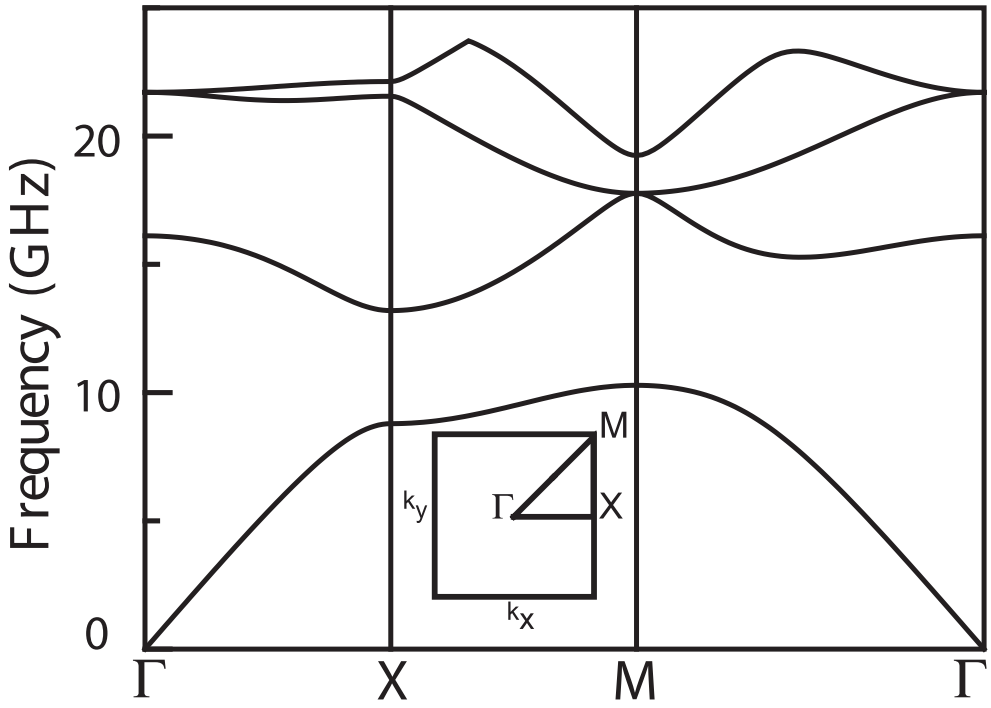

Figure 3.3: Band structure of the corresponding infinite photonic crystal. The first four TM polarized bands have been calculated by plane wave expansion.

photonic band structure and the corresponding eigenvectors are calculated by plane wave expansion method. Figure 4.1 shows the photonic band structure of the corresponding infinite photonic crystal for the first four TM polarized (Electric field is parallel to the axis of the rods) bands. According to the band structure calculations the lower band edge of the first band gap along $\Gamma - X$ is at 8.70 GHz and, the upper band edge of the first band gap along $\Gamma - X$ is at 13.20 GHz.

We have measured the transmission properties and the photon lifetime of the PC along $\Gamma - X$ direction. The transmission measurement (Fig. 4.2(a)) indicates that the lower edge of the first band gap along $\Gamma - X$ direction is around 8.7 GHz and the upper edge is around 13.2 GHz. These values are in agreement with the photonic band structure (Fig. 4.1). The measured photon lifetimes around the lower band edge and the upper band egde are shown in Fig. 4.2(b) and Fig. 4.2(c), respectively. As shown in both figures, the delay time significantly increases near the band edges. The photon lifetime near the lower edge is 12.9

nsec, which is 14× larger than the time required for the EM waves to propagate along the structure (0.92 nsec). So, the PC reduces the group velocity of light at this frequency by a factor of 14. For the upper edge, the lifetime is 19.2 nsec, which corresponds to a 22 times reduction for the speed of light.

The enhancement factor for the EM waves emitted from a monopole source along $\Gamma - X$ direction is measured for various source locations inside the center cell of the photonic crystal. The enhancement factor is defined as the ratio of the intensity of the EM waves emitted from a source located inside the photonic crystal to the intensity of the EM waves emitted from a source in free space. Figures 4.3(a) and 4.3(b) show the enhancement factors measured at various source locations inside the center unit cell for frequencies near the lower edge and the upper edge, respectively. The source locations are shown in Fig. 4.3(c). Although enhancement of radiation is expected for the band edge modes, the enhancement factor is not the same at all of the source locations. The enhancement factors presented in Fig. 4.3(a) and Fig. 4.3(b) show that the enhancement factor decreases for the lower band edge and increases for the upper band edge as we move the source away from the center rod. This can be explained by the fact that the emission of radiation depends on the intensity of the modes at the source location. The modes of the lower band edge are dielectric modes, while the modes of the upper band edge are air modes. Hence, as we move the source away from the center rod, LDOS and correspondingly, the enhancement factor is expected to decrease for the lower band edge and increase for the upper band edge. We also observe that the maximum enhancement factor for the upper band edge is higher than the enhancement factor for the lower band edge. This can be attributed to two major factors. First, for the lower band edge the electric field intensity of the mode is high inside the high dielectric material. Since the high dielectric region of the photonic crystal is not experimentally accessible, the possible highest enhancement factor can not be measured for the lower band edge. Second, the higher bands are flatter than the lower bands. This results in lower group velocities for the upper band edge for a finite photonic crystal [56]. Hence, we expect LDOS and enhancement factor to be higher for the upper band edge when compared to the lower band edge.

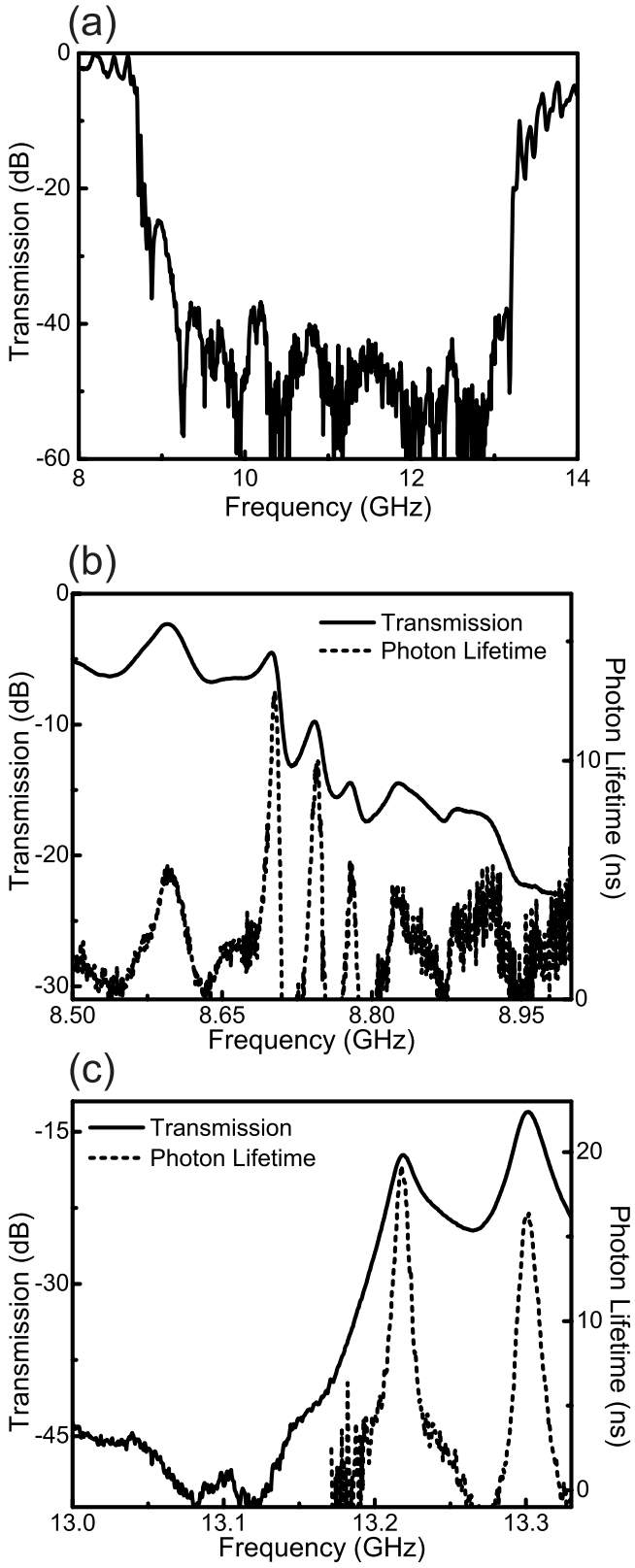

Figure 3.4: a) Transmission along $\Gamma - X$ between 8 GHz and 14 GHz. b) Solid curve represents transmission and dashed curve represents photon lifetime for the lower band edge along $\Gamma - X$ direction. c) Solid curve represents transmission and dashed curve represents photon lifetime for the upper band edge along $\Gamma - X$ direction.

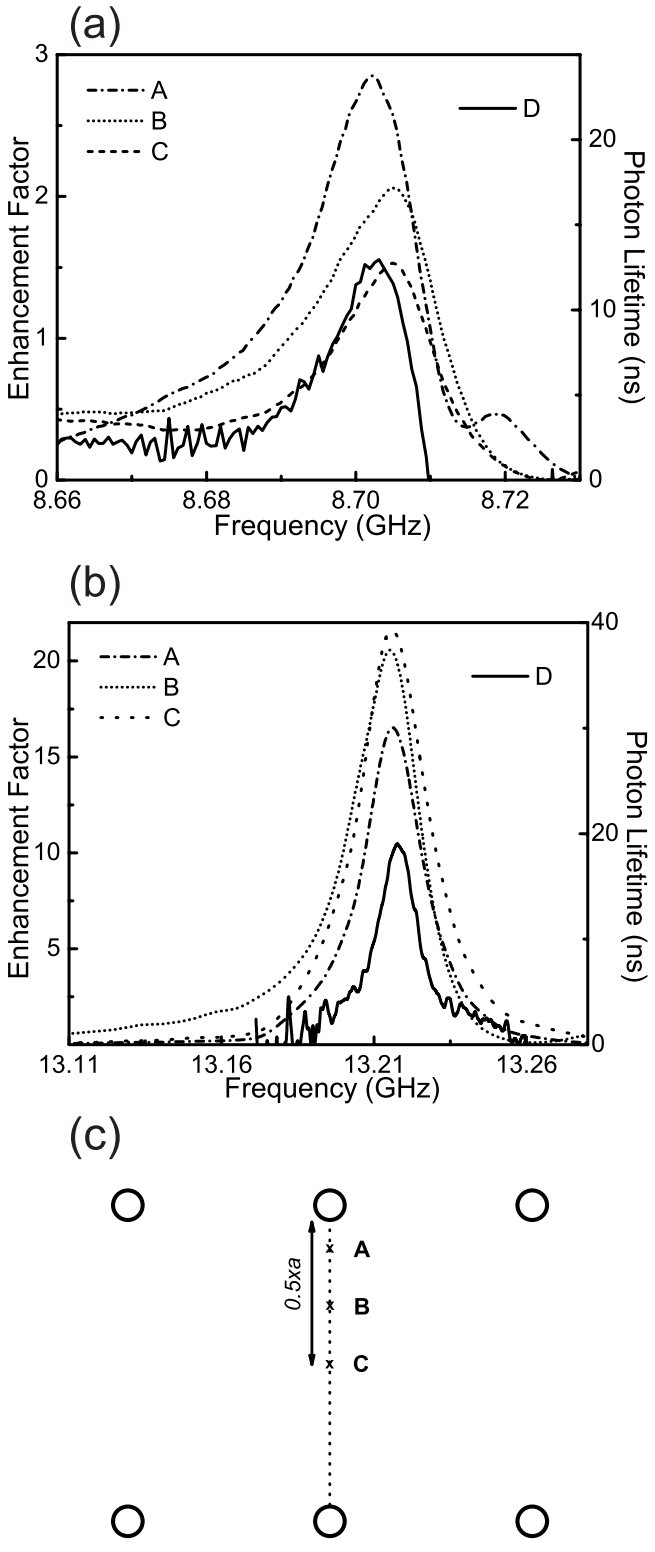

Figure 3.5: a) Enhancement factor near the lower band edge along $\Gamma - X$ for a source located at A: $0.1 \times a$, B: $0.3 \times a$,C: $0.5 \times a$ away from the center rod. D: represents the measured photon lifetime b) Enhancement factor near the upper band edge along $\Gamma - X$ for a source located at A: $0.1 \times a$, B: $0.3 \times a$,C: $0.5 \times a$ away from the center rod. D: represents the measured photon lifetime c) A, B, and C show the source locations that are used in Figures 4.3(a) and 4.3(b).

Photonic band structure (Fig. 4.1) shows that at the lower band edge frequency along $\Gamma - X$ direction there are modes along other propagation directions, such as the equal frequency mode along $\Gamma - M$ direction. So, a monopole source placed inside the photonic crystal can also radiate into these other modes. On the other hand, at the band edge frequency along $\Gamma - M$ direction, there are no such equal frequency modes along different propagation directions. Hence, we expect to observe higher enhancement factors for the frequencies near the lower band edge along $\Gamma - M$ when compared to $\Gamma - X$ direction. We experimentally check this argument by measuring the enhancement factor near the lower edge of the first band gap along $\Gamma - M$ direction. The lower edge along $\Gamma - M$ direction is around 10.15 GHz (Fig. 4.4). Figure 4.5 shows the enhancement factor along $\Gamma - M$ for various source locations inside the center cell of the photonic crystal around 10.15 GHz. A maximum enhancement factor of 4.2 is observed at the lower band edge frequency along $\Gamma - M$ direction, which is higher than the maximum enhancement factor measured for $\Gamma - X$ direction.

3.2.3 Monopole Inside a Cavity

In the previous discussions, we have emphasized the dependence of LDOS and enhancement factors on the intensity of the modes at the source locations and on the group velocities of the modes. In this sense, single cavity structures are promising structures for the control of emission from radiation sources, as the intensity of the cavity mode is localized and the group velocity for the cavity mode is reduced. Single cavity structures have been investigated by several authors [3, 4, 5, 6, 7]. A variety of applications utilizing cavity structures have been proposed, such as single-mode light-emitting diodes [57], resonant antennas [58], optical filters [59] and resonant cavity enhanced detectors [60].

We have removed the center rod from a 9×9 square array of alumina rods to create the single cavity structure. The measured transmission and the delay data for the single cavity structure are shown in Fig. 3.8(a). The transmission data indicates that the defect mode is around 11.6 GHz with a peak transmission of 0.025. The photon lifetime measurement shows an increase in the photon lifetime

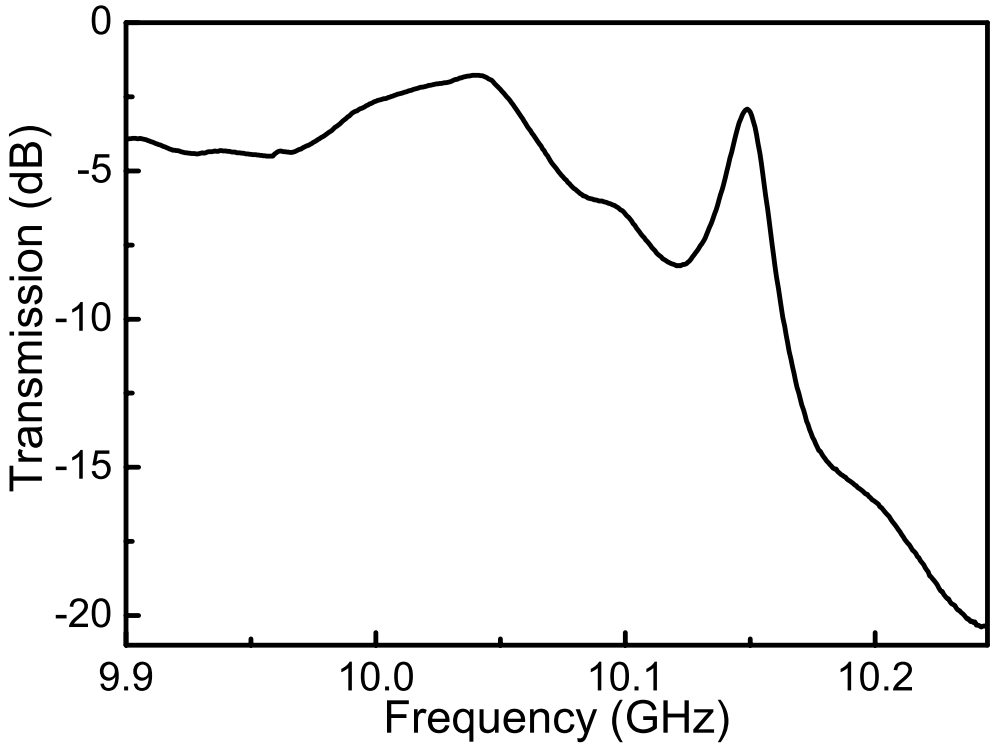

Figure 3.6: Solid curve represents the transmission along $\Gamma - M$ direction.

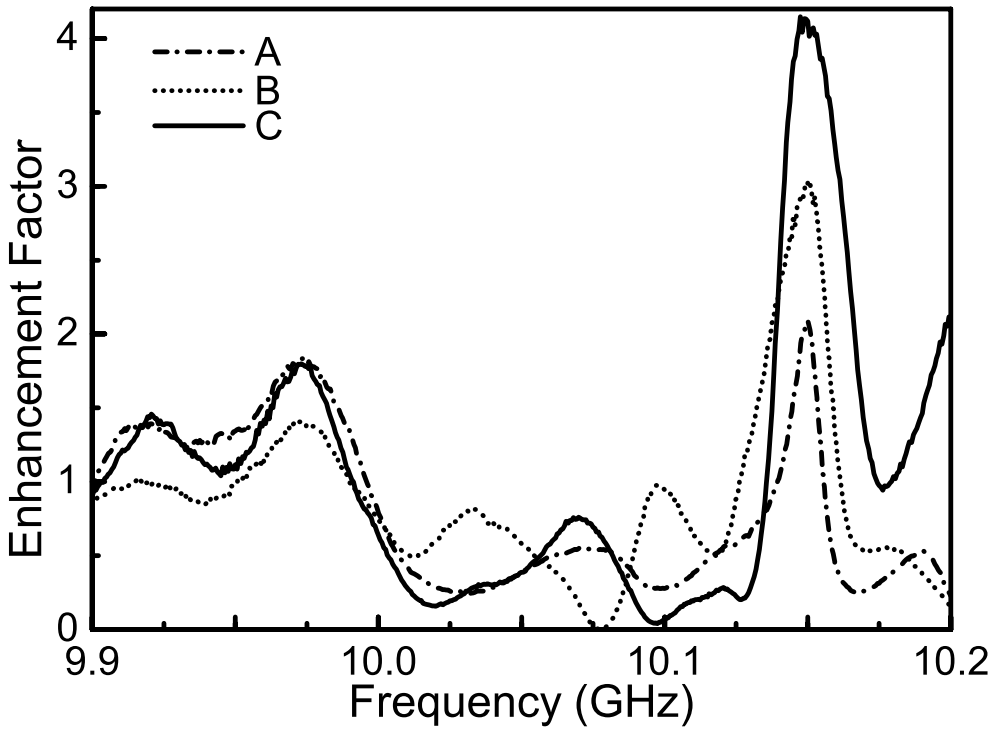

Figure 3.7: Enhancement factor near the lower band edge along $\Gamma - M$ for a source located at A: $0.5 \times a$, B: $0.3 \times a$,C: $0.1 \times a$ away from the center rod.

by a factor of 48. This also means that at the defect mode the group velocity is 48 times smaller when compared to the electromagnetic waves propagating in free space. In addition to the reduced group velocity, the computed mode profile in Fig. 3.8(b) shows that the intensity of the cavity mode is localized inside the cavity. Hence, at the cavity mode we expect to observe high enhancement factors for a monopole source located inside the cavity. Figure 3.9(a) shows the measured enhancement factor along $\Gamma - X$ direction for various source locations inside the cavity. Enhancement factor measurements for the cavity structure show that as we move the source towards the center of the cavity, the cavity frequency shifts to higher frequencies. This is due to the modification of the cavity by the finite size of the radiation source. We also observe that as we move the source towards the center, the enhancement factor for the corresponding cavity mode increases. Maximum enhancement factor is obtained when the source is located at the center of the cavity. This can be explained by the LDOS picture. Since the intensity of the cavity mode increases towards the center of the cavity, LDOS is expected to increase as we move the radiation source towards the center of the cavity.

3.2.4 Monopole Inside Coupled Cavity Structure

Coupled Cavity (CC) structures have been investigated by many authors for their waveguiding properties [8, 9, 10, 11, 12, 13]. These structures provide a novel mechanism for electromagnetic wave propagation. In CC structures, the mechanism for electromagnetic wave propagation is the hopping of photons due to the interaction between the neighboring evanescent cavity modes [48]. For CC structures, reduced group velocities for the CC modes have been reported [48]. Also the electric field intensity of CC modes are localized in the coupled cavities.

The CC structure that we have used for our experiments is created by introducing 10 single cavities to the 11^{th} column of a 21×21 square array of alumina rods. A single cavity is obtained by removing one rod from the perfect crystal. Each cavity is separated from the neighboring cavity by one rod. Figure 3.10(b) shows the details of the CC structure. The transmission and photon lifetime data presented in Fig. 3.10(a) shows that there are 10 cavity modes, which are equal

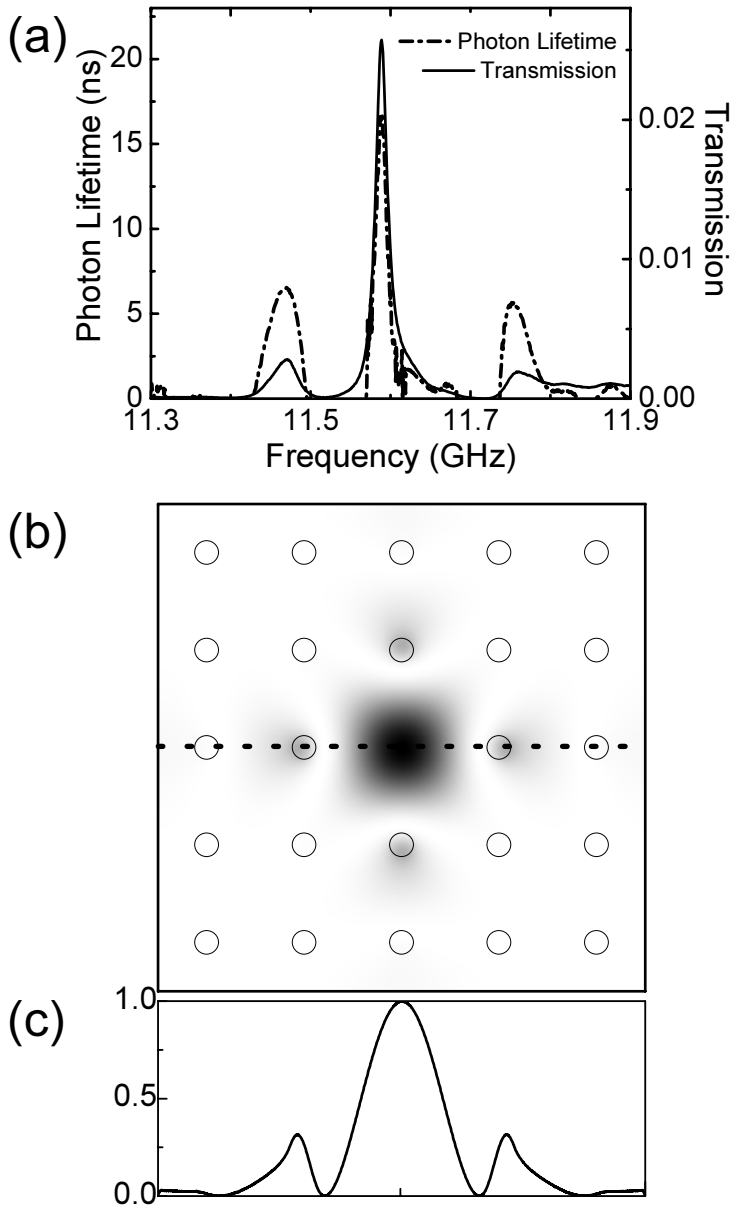

Figure 3.8: a) Solid curve represents transmission and dashed curve represents photon lifetime for the cavity mode. b) Contour plot of electric field intensity for the cavity mode. Electric field intensity has been calculated by plane wave expansion method. A 5×5 supercell has been used in the calculation. c) Intensity of the electric field for the cavity mode along the cross section shown with dotted line in Fig. 3.8(a)

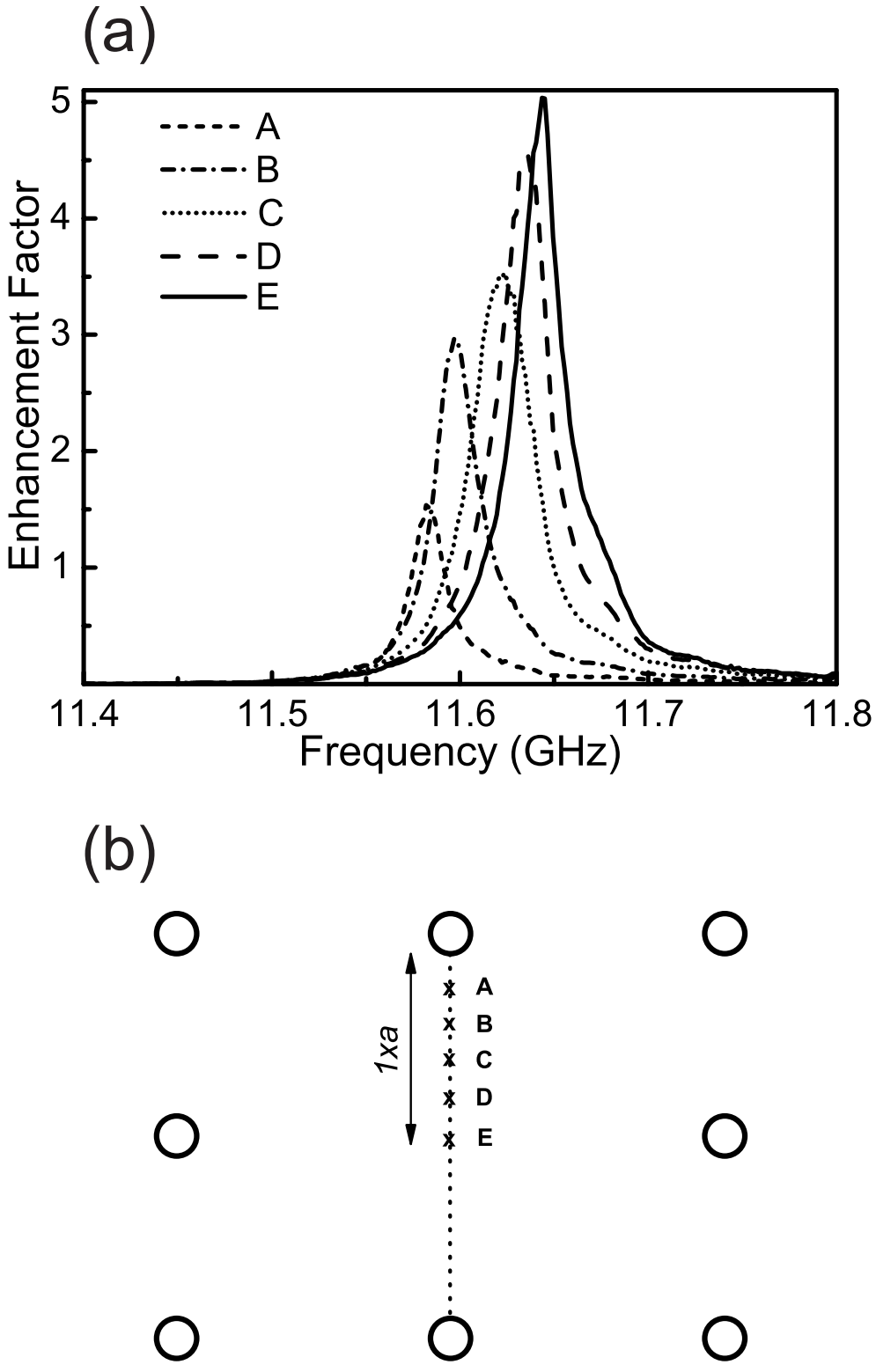

Figure 3.9: a) Enhancement factor for a source located inside a cavity A: $0.2 \times a$, B: $0.4 \times a$, C: $0.6 \times a$, D: $0.8 \times a$, E: $1 \times a$ away from the rod. b) A, B, C, D, and E show the source locations that are used in Fig. 3.9(a)

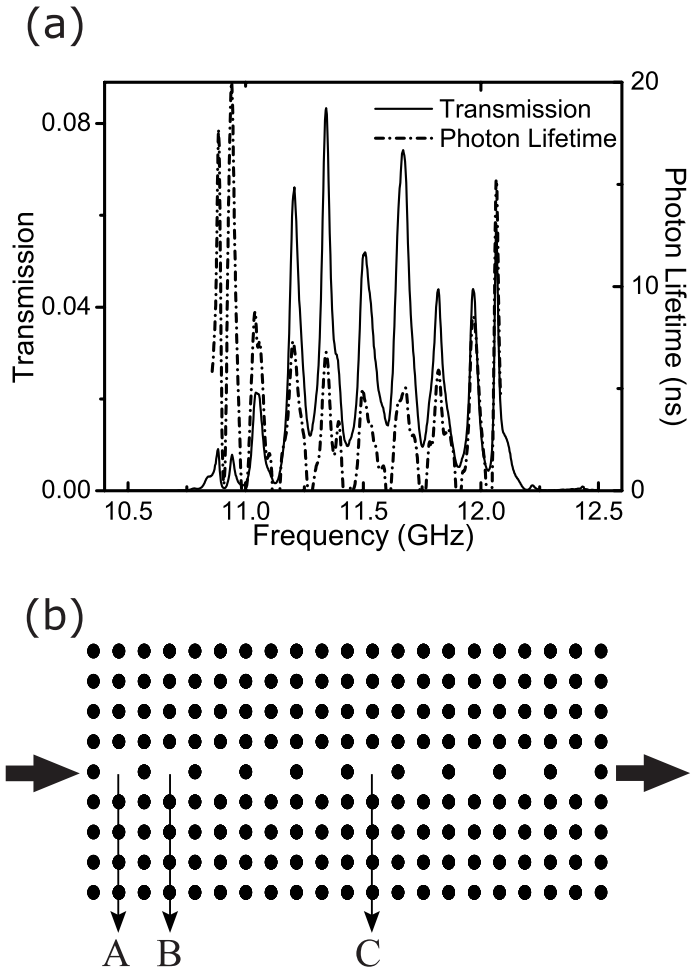

Figure 3.10: a) Solid curve represents transmission and dashed curve represents photon lifetime for the coupled cavity structure. b) Schematics of coupled cavity structure.

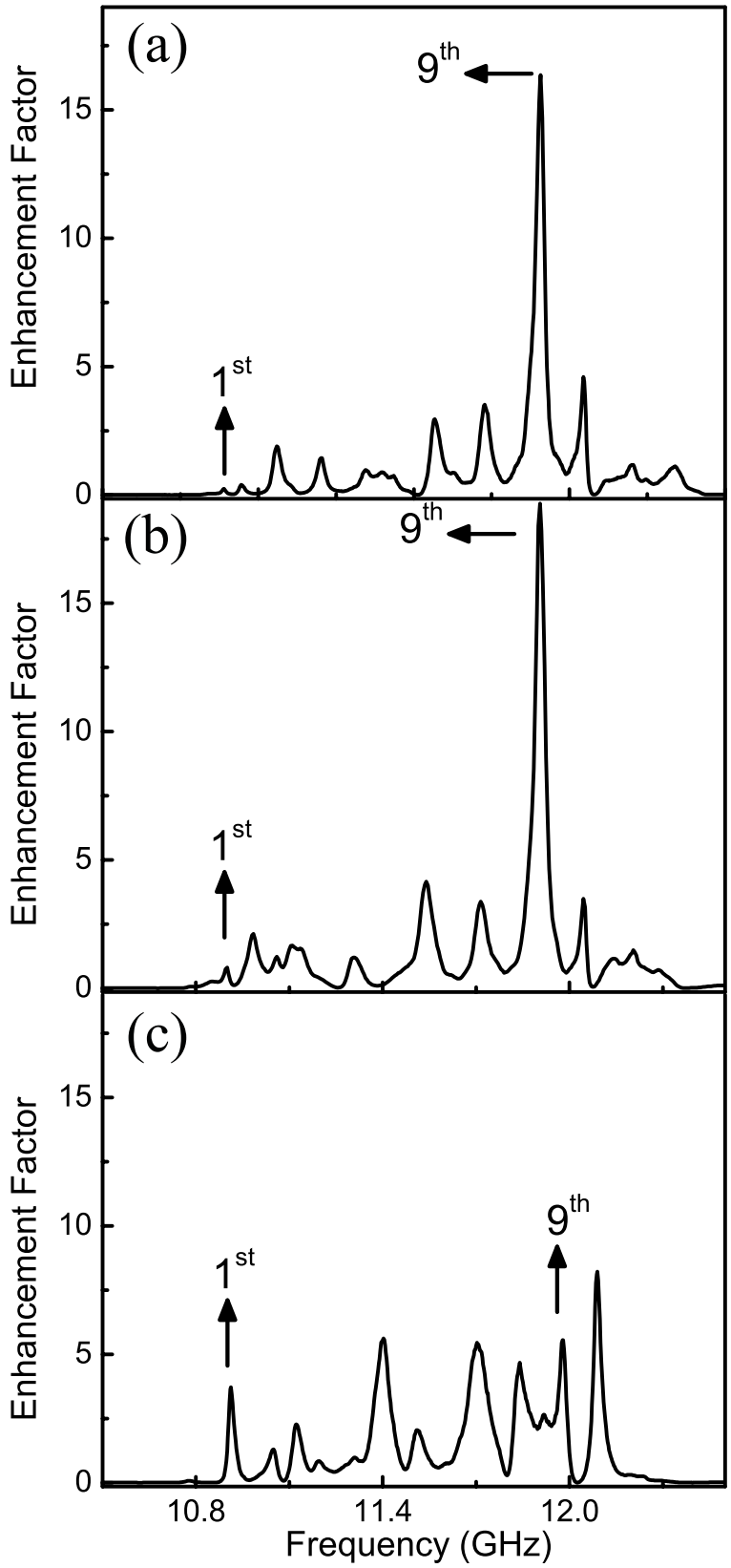

Figure 3.11: Enhancement factor for a source located at the center of a) cavity A, b) cavity B and c) cavity C.

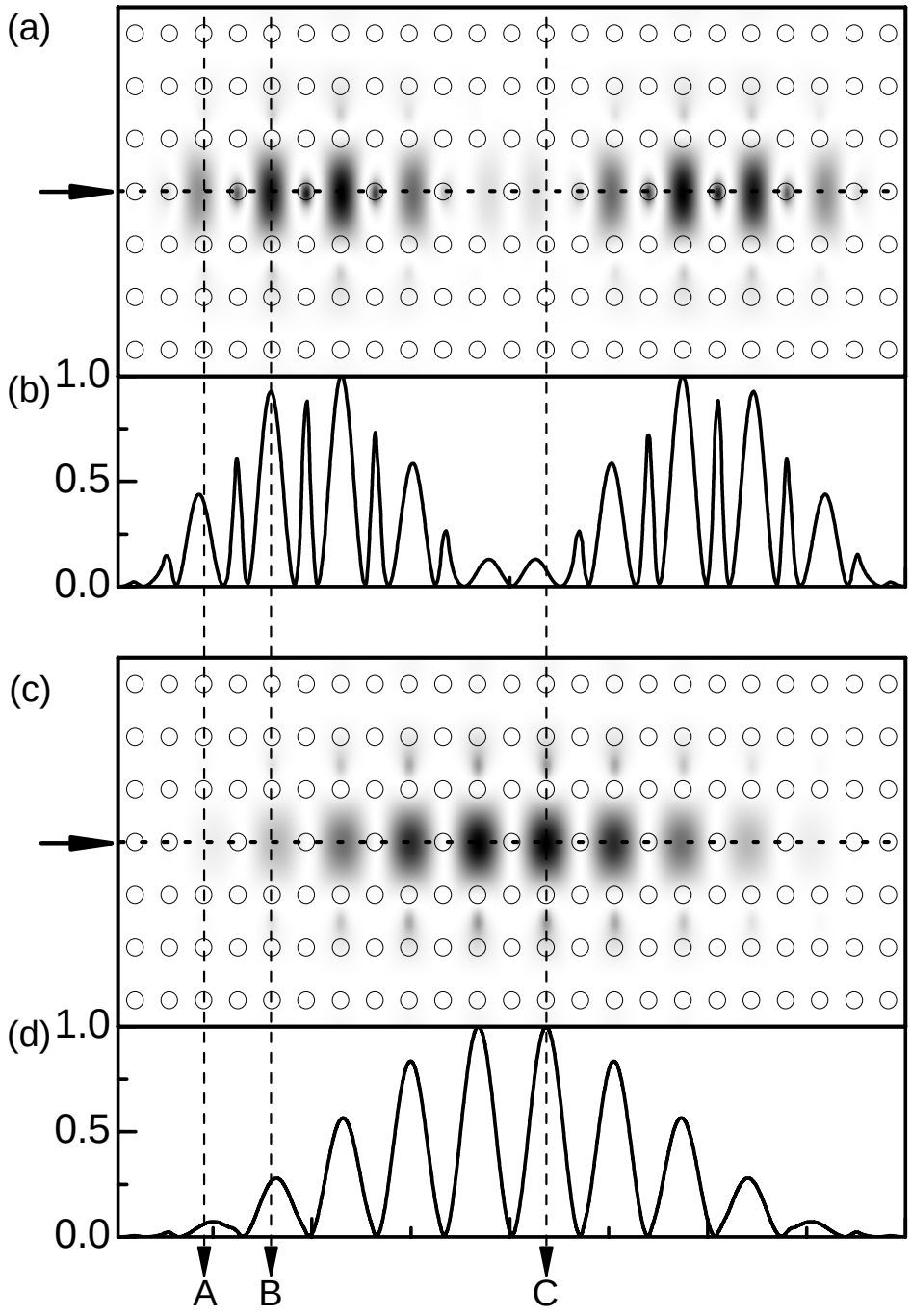

Figure 3.12: a) Contour plot of electric field intensity for the 9^{th} CC mode. Electric field intensity was calculated by plane wave expansion method using a 23×5 supercell. b) Electric field intensity for the 9^{th} CC mode along the cross section shown with dotted line in Fig. 3.12(a). The cross section is along the direction of propagation and crosses the perpendicular direction at the center of the cavities. c) Contour plot of the electric field intensity for the 1^{st} CC mode. d) Electric field intensity for the 1^{st} cavity along the cross section shown with dotted line in Fig. 3.12(c). The cross section is along the direction of propagation and crosses the perpendicular direction at the center of the cavities.

Table 3.1: Measured enhancement factors at the 1^{st} and 9^{th} CC modes for a source placed at the center of cavities.

	Cavity A	Cavity B	Cavity C
1^{st} mode	0.24	0.80	3.72
9^{th} mode	16.30	18.80	5.55

to the number of cavities. At the CC modes, transmission is high compared to the transmission through the photonic crystal without the coupled cavities. Transmissions as high as 10% have been observed at the CC modes. We also observe that the photon lifetime is increased at the CC modes. The increase in the photon lifetime indicates that the group velocities of the CC modes are reduced when compared to the EM waves propagating in free space. For the first two CC modes (CC modes are numbered in order of increasing frequency), we observed relatively low transmission compared to other CC modes. This low transmission indicates that coupling to these modes is poor.

Due to the strong interaction between the cavities, CC structures drastically modify the spontaneous emission of radiation. We measured the enhancement factor when the monopole source is located at the center of the 1^{st} cavity (cavity A), the 2^{nd} cavity (cavity B), and the 6^{th} cavity (cavity C). The measured enhancement factors when the source is placed at the center of cavity A, cavity B, and cavity C are shown in Fig. 3.11(a), Fig. 3.11(b), and Fig. 3.11(c), respectively. The enhancement factors for the 1^{st} and 9^{th} CC modes are given in table 3.1. We observe that when the source is placed either at cavity A or cavity B, 9^{th} CC mode has highest enhancement factors, while the 1^{st} CC mode has the lowest enhancement factor compared to the other CC modes. At cavity A and cavity B, enhancement factors of 16.3 and 18.8 have been observed respectively (Table 3.1). On the other hand, Fig. 3.11(c) and table 3.1 show that when we place the source at cavity C, the enhancement factor for the 1^{st} CC mode is higher for cavity C, when compared to cavities A and B. This can be explained by the fact that the enhancement factor depends on the intensity of electric field at the source location. Since the intensity of the electric field for the 9^{th} CC mode shown in Fig. 3.12(a) and Fig. 3.12(b) is high at the centers of cavity A and cavity B, we expect higher enhancement factors for this CC mode when the source is

placed at cavity A or cavity B. On the other hand, intensity of the electric field for the 1^{st} CC mode shown in Fig. 3.12(c) and Fig. 3.12(d) is high at the center of cavity C. Hence, when we place the source at cavity C, we expect 1^{st} mode to have a higher enhancement factor compared to the enhancement factors obtained for this mode when the source is placed at either cavity A or cavity B.

In summary, in this chapter we studied the emission of radiation from a monopole source located inside a photonic crystal and inside various defect structures created in a photonic crystal. We showed the enhancement of radiation along with reduced group velocities at the band edges. Moreover, we experimentally demonstrated the enhancement of radiation at a single cavity mode and at the CC modes. At the single cavity and CC modes, low group velocities along with high electric field intensities result in increased enhancement factors. In conclusion, enhancement factor for a source depends on the group velocity of the mode and on the intensity of the electric field at the source location.

Chapter 4

Highly directive radiation

4.1 Introduction

In the previous chapter we have showed that it is possible to use photonic crystals to enhance the emission of radiation from localized sources. In this chapter we will examine the possibility of using photonic crystals to confine the emitted power to a narrow angular region. We will be particularly interested in the modes near the upper band edge of the first band gap. These modes are important since if we can show that the emitted power near these modes are confined to a narrow angular region we would then have solved the problem of control of emission.

Photonic crystals have been used, especially in the antenna community, to improve the angular confinement of power from radiation sources [61, 62, 63, 64, 65, 66]. In most of these works the sources are not inside the PCs and PCs have been used either as a cover or a substrate [61, 62, 63, 64].

We will study the angular distribution of power from a radiation source embedded inside a PC and we will show that it is possible to confine the emitted power to a very narrow angular region at certain frequencies. Moreover, we will show that the size of the PC is a critical parameter. This chapter will be organized as follows: we will first discuss the properties of PCs relevant to our study

and then we will present our experimental and theoretical results.

4.2 Discussion

One of the points we will use in our discussion is the band structure of the PC used in our study. The PC that we used in our experiments and calculations is the same as that we used in chapters 2 and 3. Band structure of the corresponding infinite PC in the whole first Brillouin zone for TM-polarized EM waves is given in Fig. 4.1. Throughout this chapter we consider only TM-polarized EM waves. From the band structure we observe that at the upper band edge (the minimum of the second band) only the modes along $\Gamma - X^{'}$, where $X^{'}$ represents all directions having the same symmetry properties of X point, are allowed to propagate inside the PC. For the modes near the upper band edge $k_{\parallel} = k_x \approx 0$. Since apart from an additive reciprocal lattice vector, $k_{\parallel}$ is conserved at the air-PC interface, section 2.3, we conclude that for a source embedded inside the PC and operating at the upper band edge frequency, the emitted waves should be appreciably transmitted from the PC to air only along $\Gamma - X$ direction. In addition, the modes near the upper band edge are air modes, i.e., most of the energy of the EM waves are concentrated in the low dielectric material region as the waves propagate through the PC (Fig.4.2 - (a)). Hence, when the waves near the upper band edge emerge from the surface of the PC, most of the power will flow through low dielectric material region of the PC (Fig. 4.2 - (b)). In conclusion, we can regard the exit points as radiation sources.

In section 2.1.4 we have shown that the group velocities for the modes near the band edges are fairly reduced compared to the group velocity of EM waves propagating in free space. Delay time measurements presented in Fig. 4.3 show that the group velocities for the modes near the upper band edge are reduced up to 22 times in comparison to air. Delay time is defined as $\tau_p = \partial\varphi/\partial\omega$ [44]. Here, φ is the net phase difference between the phase of the EM wave propagating inside the photonic crystal and the phase of the EM wave propagating in free space. The reduced group velocities at the upper band edge result in phase differences

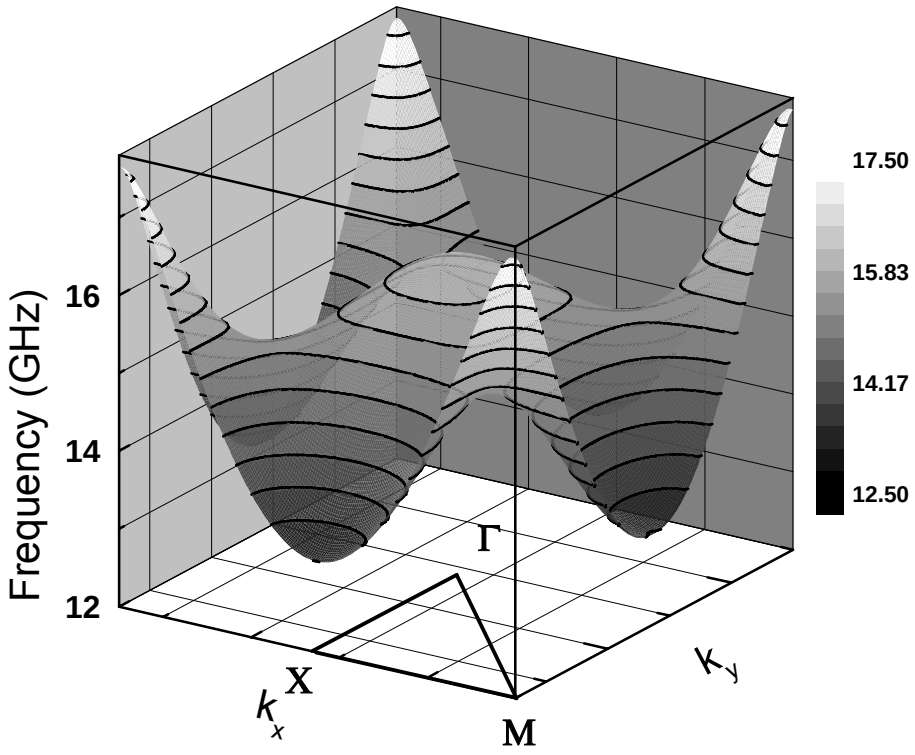

Figure 4.1: The second TM polarized band is shown over the whole first Brillouin zone.

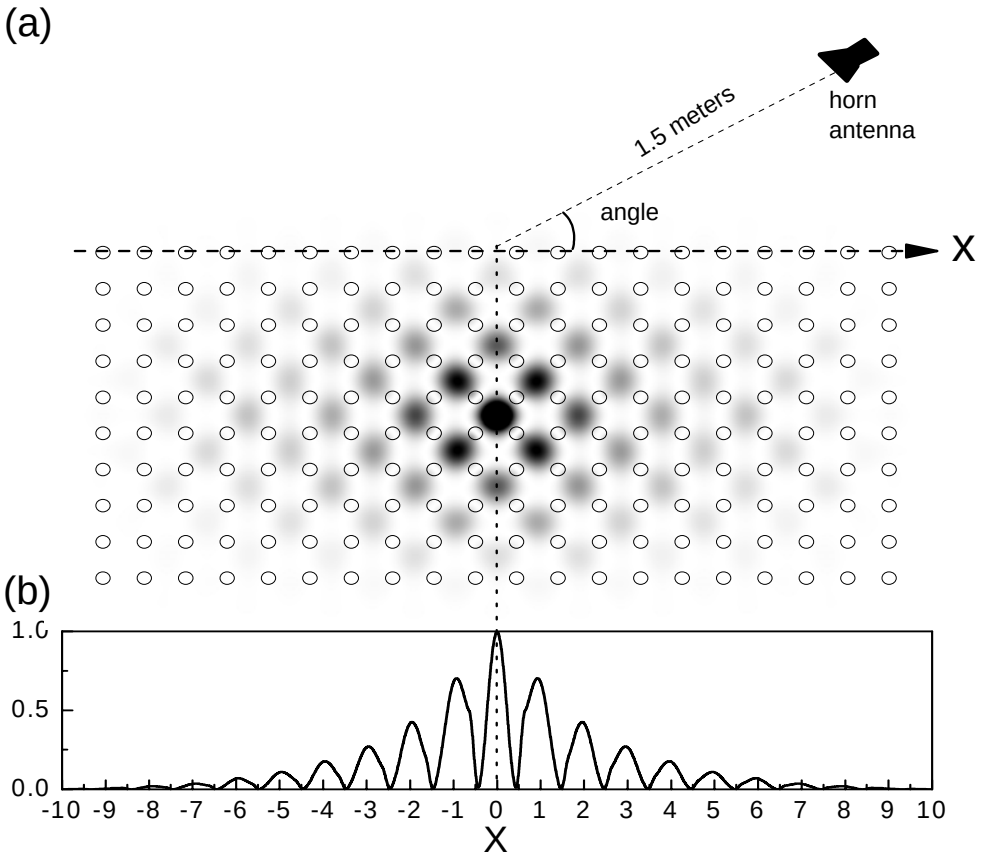

Figure 4.2: (a) Experimental configuration for a 2D 20×10 square array. The source is at the center of the PC. Also, the contour plot of the electric field intensity for a source radiating at the band edge frequency is shown. Electric field intensity is mostly localized in air. (b) Electric field intensity along X axis.

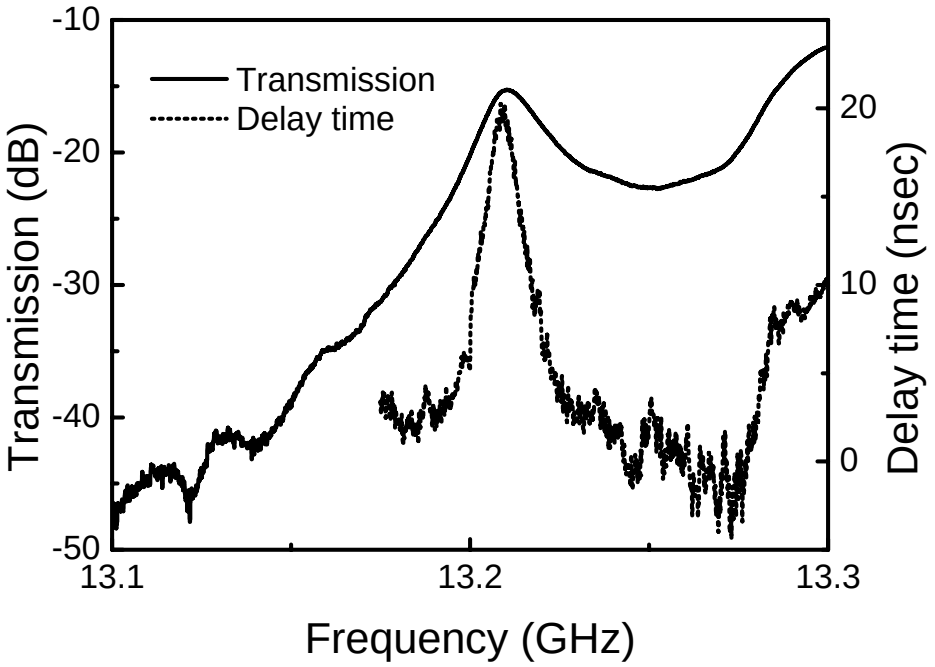

Figure 4.3: Measured transmission and delay time near the upper band edge for the PC used in our experiments.

between the radiators. Since at the upper band edge the modes are allowed to propagate only along $\Gamma - X'$, these radiation sources will have a uniform distribution of phase differences.

Combining the results of the discussions of the previous paragraphs, we conclude that the surface of the PC can be regarded as a system of radiation sources. All of these sources operate at the upper band edge frequency and have similar spatial and temporal distribution of power with a uniform phase difference between the radiators. This system of radiators is similar to an antenna array. Since all the radiators of the system radiate in $\Gamma - X$ direction, we expect the emitted power from a source embedded inside the PC to be confined to a narrow angular region.

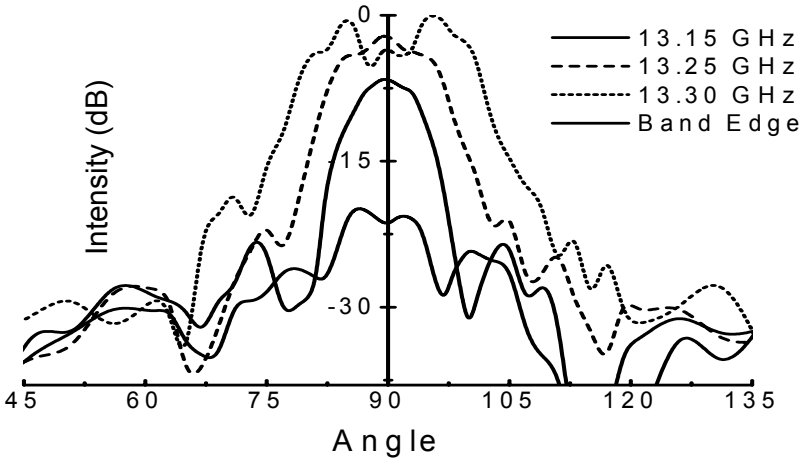

Figure 4.4: Measured far field radiation patterns for various frequencies near the upper band edge. The crystal size is 32×16.

4.3 Experiments and results: highly directive radiation at the band edge

In our experiments and FDTD calculations, we calculated and measured the angular distribution of power emitted from a monopole source embedded inside a 2D square array of cylindrical alumina rods. The monopole source used in the experiments is obtained by removing 0.5 cm of the cladding from a coaxial cable and leaving the central conductor, fig. 3.2. An HP-8510C network analyzer is used to excite the monopole source and to measure the power emitted from the monopole source. Figure 4.2 shows the details of experimental configuration.

We carried out the measurements and the calculations for various frequencies and for various crystal lengths. Crystal length is defined as the number of layers along x axis. Since the PC used in experiments is a 2D structure, we are interested in the angular distribution of power on the plane perpendicular to the axis of the rods. The measured far field radiation patterns for a square array of 32×20 alumina rods at various frequencies near the upper band edge are presented in Fig. 4.4. The minimum half power beam width is obtained at 13.21 GHz and it

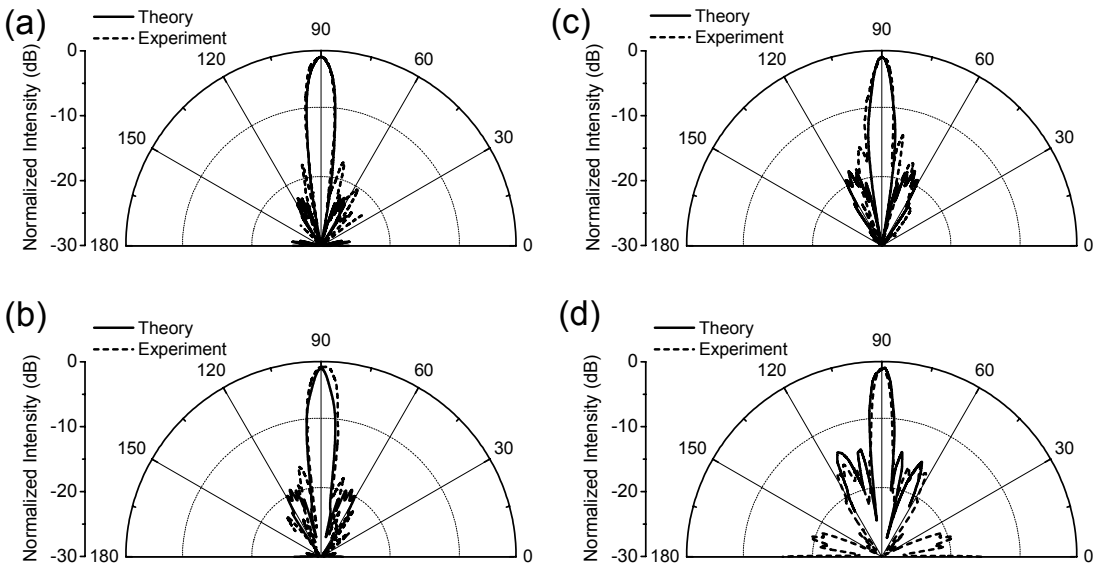

Figure 4.5: Measured and calculated far field radiation patterns at the upper band edge frequency for various crystal lengths. (a) 32×16 layers (b) 28×16 layers (c) 24×16 layers (d) 20×16 layers.

is found to be 8°. The measured delay time data presented in Fig. 4.2 shows that the maximum delay time occurs at 13.21 GHz. Comparing the delay time data with the band structure of the corresponding infinite PC we conclude that the upper band edge is at 13.21 GHz. Hence, the minimum half power beam width is obtained at the upper band edge frequency. Figure 4.4 shows that the angular distribution of power strongly depends on the radiation frequency. The radiation patterns are wider for frequencies higher than the upper band edge frequency. This can be explained by the presence of equal frequency modes along different directions at frequencies higher than the upper band edge frequency.

We have also measured the angular distribution of power at the upper band edge frequency for various crystal lengths. The measured and calculated far field radiation patterns are presented in Fig. 4.5. We have measured half power beam widths of 8°, 7°, 6°, and 12° for crystal lengths of 32, 28, 24, and 20, respectively. The measured half power beam widths show that there is an optimum crystal length, which is found to be 24 layers in our case. The minimum half power beam width is obtained for 24 layers and it is found to be 6°. From Fig. 4.5 and

the measured half power beam widths we also observe that as the crystal length is changed from its optimum value, radiation patterns and half power beam widths also change. The change is more significant when the layer number is decreased from its optimum value. This can be explained by the fact that the strength of the radiators decreases rapidly as we move away from the center of the PC (Fig. 4.2 - (b)). Hence, the effect of increasing the crystal length on the radiation patterns is less significant when compared to the effect of decreasing the crystal length.

4.4 Conclusion

In summary, we have demonstrated that by using PCs it is possible to confine the emitted power to a narrow angular region for a source embedded inside a PC and radiating at the band edge frequency. A minimum half power beam width of 6° have been obtained for a source operating at the upper band edge frequency of the PC. This is the minimum experimental value obtained from sources based on PCs. Our results also show that the far field radiation pattern of an antenna embedded inside a PC strongly depends on the frequency and on the crystal size. The findings of our work can be used to improve the performance of certain devices such as antennas and LED's.

Chapter 5

Conclusions and Future Work

This chapter includes a brief summary of previous chapters and the results of this thesis work. In addition, we will briefly mention about the new questions and possible future work that our results lead us to.

In the second chapter we had a somewhat long discussion about the theory of photonic crystals and the dipole radiation in photonic crystals. We showed that the periodic dielectric constant arrangement leads to the concept of frequency bands. A method to calculate these bands was derived. Then, we encountered the problem of dipole radiation in photonic crystals. We showed that the dipole radiation is inversely proportional to the group velocity of the modes, and it is proportional to the electric field intensity of the modes at the source location.

The main objective of this thesis work can be stated as *to control the emission of radiation*. The word *control* basically includes two major aspects: to enhance the radiation and to confine the emitted power to a narrow angular region. In this respect we studied the emission of radiation from a monopole source embedded inside a photonic crystal. In the third chapter, our experimental and theoretical results showed that the emitted power can be enhanced as much as 22 times at the upper band edge of the first band gap for the photonic crystal that we considered. Moreover, we studied monopole radiation inside certain defect structures built in photonic crystals. Our results showed that monopole radiation is also enhanced in

defect structures. It should be noted that our results showed striking correlation between the delay time and enhancement, also a striking correlation between the electric field intensity and the enhancement. Since we obtained a very high enhancement at the upper band edge we studied the angular distribution of power near these modes. The results of our angular distribution studies are summarized in the fourth chapter. We found that interestingly angular confinement is achieved just at the upper band edge. The measured half power beam width at the upper band edge was found to be 6 degrees, which is the smallest value in the literature obtained by using photonic crystals. The results of this thesis work can be stated as *by using photonic crystals control of emission of radiation is possible.*

The results of this thesis work lead us to some interesting questions. For instance, we achieved angular confinement by using photonic crystals. But is it possible to direct the emitted power to a certain point in space without mechanically altering the system? Another interesting question is the temporal behavior of sources inside photonic crystals. Are the decay rates exponential? We will try to answer these questions in our future work. For $2D$ photonic crystal vertical loss is a big problem. To solve this we will consider $3D$ photonic crystals.

Bibliography

[1] K. Ohtaka, "Energy band of photons and low-energy photon diffraction," *Phys. Rev. B* **19**, pp. 5057–5067, 1979.

[2] J. D. Joannopoulos, R. D. Meade, and J. N. Winn, *Photonic Crystal: Molding the Flow of Light*, Princeton University Press, Princeton, NJ, 1995.

[3] E. Ozbay, G. Tuttle, M. Sigalas, C. M. Soukoulis, and K. M. Ho, "Defect structures in a layer-by-layer photonic band-gap crystal," *Phys. Rev. B* **51**, p. 13961, 1995.

[4] M. M. Sigalas, K. M. Ho, R. Biswas, and C. M. Soukoulis, "Theoretical investigation of defects in photonic crystals in the presence of dielectric losses," *Phys. Rev. B* **57**, p. 3815, 1998.

[5] J. M. Smith, R. M. D. L. Rue, M. Rattier, S. Olivier, H. Benisty, C. Weisbuch, and T. F. Krauss, "Coupled guide and cavity in a two-dimensional photonic crystal," *Appl. Phys. Lett.* **78**, p. 1487, 2001.

[6] T. Ochiai and J. Sánchez-Dehesa, "Localized defect modes in finite metallic two-dimensional photonic crystals," *Phys. Rev. B* **65**, p. 245111, 2002.

[7] S. Lan, S. Nishikawa, Y. Sugimoto, N. Ikeda, K. Asakawa, and H. Ishikawa, "Analysis of defect coupling in one- and two-dimensional photonic crystals," *Phys. Rev. B* **65**, p. 165208, 2002.

[8] N. Stefanou and A. Modinos, "Impurity bands in photonic insulators," *Phys. Rev. B* **57**, p. 12127, 1998.

[9] A. Yariv, Y. Xu, R. K. Lee, and A. Scherer, "Coupled-resonator optical waveguide: a proposal and analysis," *Opt. Lett.* **24**, p. 711, 1999.

[10] M. Bayindir, E. Cubukcu, I. Bulu, and E. Ozbay, "Photonic band-gap effect, localization, and waveguiding in the two-dimensional penrose lattice," *Phys. Rev. B* **63**, p. 161104, 2001.

[11] S. Lan, S. Nishikawa, H. Ishikawa, and O. Wada, "Design of impurity band-based photonic crystal waveguides and delay lines for ultrashort optical pulses," *J. Appl. Phys.* **90**, p. 4321, 2001.

[12] M. Bayindir, B. Temelkuran, and E. Ozbay, "Propagation of photons by hopping: A waveguiding mechanism through localized coupled cavities in three-dimensional photonic crystals," *Phys. Rev. B* **61**, pp. R11855–R11858, 2000.

[13] V. Yannopapas, A. Modinos, and N. Stefanou, "Waveguides of defect chains in photonic crystals," *Phys. Rev. B* **65**, p. 235201, 2002.

[14] E. Yablonovitch, "Inhibited spontaneous emission in solid-state physics and electronics," *Phys. Rev. Lett.* **58**, p. 2059, 1987.

[15] I. Bulu, H. Caglayan, and E. Ozbay, "Radiation properties of sources inside photonic crystals," *Phys. Rev. B* **67**, p. 205103, 2003.

[16] I. Bulu, H. Caglayan, and E. Ozbay, "Highly directive radiation from sources embedded inside photonic crystals," *accepted for publication in Applied Physics Letters* .

[17] E. M. Purcell *Phys. Rev. B* **69**, p. 681, 1946.

[18] J. M. Raimond, M. Gross, and S. Haroche, "Observation of cavity-enhanced single-atom spontaneous emission," *Phys. Rev. Lett.* **50**, pp. 1903–1906, 1983.

[19] P. Dobiasch and H. Dehmelt *Ann. Phys. (Paris)* **10**, p. 825, 1985.

[20] K. M. Ho, C. T. Chan, and C. M. Soukoulis, "Existence of a photonic gap in periodic dielectric structures," *Phys. Rev. Lett.* **65**, pp. 3152–3155, 1990.

[21] E. Ozbay, E. Michel, G. Tuttle, R. Biswas, M. Sigalas, and K.-M. Ho, "Double-etch geometry for millimeter-wave photonic band-gap crystals," *Appl. Phys. Lett.* **64**, p. 2059, 1994.

[22] E. Ozbay, "Layer-by-layer photonic crystals from microwave to far-infrared frequencies," *J. Opt. Soc. Am. B* **13**, p. 1945, 1996.

[23] A. A. Asatryan, K. Busch, R. C. McPhedran, L. C. Botten, C. M. de Sterke, and N. A. Nicorovici, "Two-dimensional green's function and local density of states in photonic crystals consisting of a finite number of cylinders of infinite length," *Phys. Rev. D* **63**, p. 046612, 2001.

[24] R. Wang, X.-H. Wang, B.-Y. Gu, and G.-Z. Yang, "Local density of states in three-dimensional photonic crystals: Calculation and enhancement effects," *Phys. Rev. B* **54**, pp. 5732–5741.

[25] Z.-Y. Li and Y. Xia, "Full vectorial model for quantum optics in three-dimensional photonic crystals," *Phys. Rev. A* **63**, p. 043817.

[26] Y. Yang and S.-Y. Zhu, "Spontaneous emission from a two-level atom in a three-dimensional photonic crystal," *Phys. Rev. A* **62**, p. 013805, 2000.

[27] Z.-Y. Li, L.-L. Lin, and Z.-Q. Zhang, "Spontaneous emission from photonic crystals: Full vectorial calculations," *Phys. Rev. Lett.* **84**, pp. 4341–4344, 1999.

[28] S.-Y. Zhu, Y. Yang, H. Chen, H. Zheng, and M. S. Zubairy, "Spontaneous radiation and lamb shift in three-dimensional photonic crystals," *Phys. Rev. Lett.* **84**, pp. 2136–2139, 2000.

[29] K. Sakoda, *Optical Properties of Photonic Crystals*, Springer-Verlag, Germany, 2001.

[30] K. Sakoda and K. Ohtaka, "Optical response of three-dimensional photonic lattices: Solutions of inhomogeneous maxwell's equations and their applications," *Phys. Rev. B* **54**, pp. 5732–5741.

[31] A. Taflove, *Computational Electrodynamics: The Finite-Difference Time-Domain Method*, Artech House INC, Norwood, 1995.

[32] K. Yee *IEEE Trans. Antennas Propag.* **14**, p. 302, 1966.

[33] V. Lousse, J.-P. Vigneron, X. Bouju, and J.-M. Vigoureux, "Atomic radiation rates in photonic crystals," *Phys. Rev. B* **64**, p. 201104, 2001.

[34] N. Vats, S. John, and K. Busch, "Theory of fluorescence in photonic crystals," *Phys. Rev. A* **65**, p. 043808, 2002.

[35] S. John and T. Quang, "Spontaneous emission near the edge of a photonic band gap," *Phys. Rev. A* **50**, pp. 1764–1769, 1994.

[36] R. Sprik, B. A. V. Tiggelen, and A. Legendijk, "Optical emission in periodic dielectrics," *Europhys. Lett.* **35**, p. 265, 1996.

[37] M. Megens, J. E. G. J. Wijnhoven, A. Lagendijk, and W. L. Vos, "Light sources inside photonic crystals," *J. Opt. Soc. Am. B* **16**, p. 1403, 1999.

[38] E. P. Petrov, V. N. Bogomolov, I. I. Kalosha, and S. V. Gaponenko, "Spontaneous emission of organic molecules embedded in a photonic crystal," *Phys. Rev. Lett.* **81**, p. 77, 1998.

[39] M. Megens, H. P. Schriemer, A. Lagendijk, and W. L. Vos, "Comment on "spontaneous emission of organic molecules embedded in a photonic crystal"," *Phys. Rev. Lett.* **83**, p. 5401, 1999.

[40] E. P. Petrov, V. N. Bogomolov, I. I. Kalosha, and S. V. Gaponenko, "Petrov et al. reply," *Phys. Rev. Lett.* **83**, p. 5402, 1999.

[41] K. Busch, N. Vats, S. John, and B. C. Sanders, "Radiating dipoles in photonic crystals," *Phys. Rev. D* **62**, p. 4251, 2000.

[42] A. G. Galstyan, M. E. Raikh, and Z. V. Vardeny, "Emission spectrum of a dipole in a semi-infinite periodic dielectric structure: Effect of the boundary," *Phys. Rev. B* **62**, p. 1780, 2000.

[43] J.-K. Hwang, H.-Y. Ryu, , and Y.-H. Lee, "Spontaneous emission rate of an electric dipole in a general microcavity," *Phys. Rev. B* **60**, pp. 4688–4695, 1999.

[44] M. Mojahedi, E. Schamiloglu, F. Hegeler, and K. J. Malloy, "Time-domain detection of superluminal group velocity for single microwave pulses," *Phys. Rev. D* **62**, p. 5758, 2000.

[45] A. M. Steinberg, P. G. Kwiat, and R. Y. Chiao, "Measurement of the single-photon tunneling time," *Phys. Rev. Lett.* **71**, p. 708711, 93.

[46] M. Scalora, J. P. Dowling, A. S. Manka, C. M. Bowden, and J. W. Haus, "Pulse propagation near highly reflective surfaces: Applications to photonic band-gap structures and the question of superluminal tunneling times," *Phys. Rev. A* **52**, p. 726734, 1995.

[47] G. DAguanno, M. Centini, M. Scalora, C. Sibilia, M. J. Bloemer, C. M. Bowden, J. W. Haus, and M. Bertolotti1, "Group velocity, energy velocity, and superluminal propagation in finite photonic band-gap structures," *Phys. Rev. D* **63**, p. 036610, 2001.

[48] M. Bayindir and E. Ozbay, "Heavy photons at coupled-cavity waveguide band edges in a three-dimensional photonic crystal," *Phys. Rev. B* **62**, pp. R2247–R2250, 2000.

[49] S. Yano, Y. Segawa, J. S. Bae, K. Mizuno, S. Yamaguchi, , and K. Ohtaka, "Optical properties of monolayer lattice and three-dimensional photonic crystals using dielectric spheres," *Phys. Rev. B* **66**, p. 075119, 2002.

[50] T. Kondo, M. Hangyo, S. Yamaguchi, S. Yano, Y. Segawa, and K. Ohtaka, "Transmission characteristics of a two-dimensional photonic crystal array of dielectric spheres using subterahertz time domain spectroscopy," *Phys. Rev. B* **66**, p. 033111, 2002.

[51] K. Ohtaka, Y. Suda, S. Nagano, T. Ueta, A. Imada, T. Koda, J. S. Bae, K. Mizuno, S. Yano, and Y. Segawa, "Photonic band effects in a two-dimensional array of dielectric spheres in the millimeter-wave region," *Phys. Rev. B* **61**, p. 5267, 2000.

[52] K. Ohtaka *J. Lightwave Technology* **17**, p. 2161, 1999.

[53] A. Imhof, W. L. Vos, R. Sprik, and A. Lagendijk, "Large dispersive effects near the band edges of photonic crystals," *Phys. Rev. Lett.* **83**, pp. 2942–2945, 1999.

[54] K. Inoue, N. Kawai, Y. Sugimoto, N. Carlsson, N. Ikeda, and K. Asakawa, "Observation of small group velocity in two-dimensional algaas-based photonic crystal slabs," *Phys. Rev. B* **65**, p. 121308, 2002.

[55] T. Aoki, M. W. Takeda, J. W. Haus, Z. Yuan, M. Tani, K. Sakai, N. Kawai, and K. Inoue, "Terahertz time-domain study of a pseudo-simple-cubic photonic lattice," *Phys. Rev. B* **64**, p. 045106, 2001.

[56] D.-Y. Jeong, Y. H. Ye, and Q. M. Zhang, "Effective optical properties associated with wave propagation in photonic crystals of finite length along the propagation direction," *J. Appl. Phys.* **92**, p. 4194, 2002.

[57] I. Schnitzer, E. Yablonovitch, A. Scherer, and T. J. Gmitter, *Photonic Band Gap and Localization*, vol. 308 of *NATO ASI SERIES B*, 1993.

[58] B. Temelkuran, M. Bayindir, E. Ozbay, R. Biswas, M. M. Sigalas, G. Tuttle, and K. M. Ho, "Photonic crystal-based resonant antenna with a very high directivity," *J. Appl. Phys.* **87**, p. 603, 2000.

[59] J. D. Joannopoulos, *Photonic Band Gap Materials*, vol. 315 of *NATO ASI SERIES E*, 1996.

[60] B. Temelkuran, E. Ozbay, J. P. Kavanaugh, G. Tuttle, and K. M. Ho, "Resonant cavity enhanced detectors embedded in photonic crystals," *Appl. Phys. Lett.* **72**, p. 2376, 1998.

[61] M. Qiu and S. He *Microwave Opt. Technol. Lett.* **30**, p. 41, 2001.

[62] R. Gonzalo, P. de Maagt, and M. Sorolla *IEE Trans. Microwave Theory Tech.* **47**, p. 2131, 1999.

[63] E. R. Brown, C. D. Parker, and E. Yablonovitch, "Radiation properties of a planar antenna on a photonic-crystal substrate," *J. Opt. Soc. Am. B* **10**, p. 404, 1993.

[64] M. P. Kesler, J. G. Maloney, B. L. Shirley, and G. S. Smith *Microwave Opt. Technol. Lett.* **11**, p. 169, 1996.

[65] S. Enoch, B. Gralak, and G. Tayeb, "Enhanced emission with angular confinement from photonic crystals," *Appl. Phys. Lett.* **81**, p. 1588, 2002.

[66] R. Biswas, E. Ozbay, B. Temelkuran, M. Bayindir, M. M. Sigalas, and K.-M. Ho, "Exceptionally directional sources with photonic-bandgap crystals," *J. Opt. Soc. Am. B* **18**, p. 1684, 2001.